


Article

Geochemical Constraints on the Evolution of Late- to Post-Orogenic Granites in the Arabian Shield, with a Specific Focus on Jabal Al Bayda Area in the Central Hijaz Region, Saudi Arabia

Hamdy H. Abd El-Naby ^{1,*} and Yehia H. Dawood ² ¹ Faculty of Earth Sciences, King Abdulaziz University, P.O. Box 80206, Jeddah 21589, Saudi Arabia² Department of Geology, Faculty of Science, Ain Shams University, Cairo 11566, Egypt; yhdawood@yahoo.com

* Correspondence: hyuosef@kau.edu.sa; Tel.: +966-5-4956-9066; Fax: +966-1-2695-2441

Abstract: The Jabal Al Bayda, located in the Hijaz terrain of northwest Saudi Arabia, comprises magmatic rocks that represent the ending phase in the Precambrian development of the Arabian Shield. Two granitic suites have been studied petrologically and geochemically, the monzogranite and alkali granite suites, to gain knowledge about their origin and geotectonic implications. The geochemical characteristics of the monzogranites align with their formation in a subduction-related environment. These rocks have a composition that is rich in strontium and barium, and low in rubidium, and displays a high-K calc-alkaline to shoshonitic nature. In contrast, alkali granites typically have lower concentrations of Sr and Ba, and higher rubidium contents. The differences in geochemical composition between monzogranites and alkali granites found in Jabal Al Bayda indicate differences in their origin and geotectonic environment. The evolution of granitoid magmatism in the Jabal Al Bayda area is linked to the Hijaz orogenic cycle, during which northwest-dipping subduction led to the formation of the Midyan, Hijaz, and Jeddah arc assemblage, followed by the collision and accretion of these arcs along the Yanbu and Bir Umq sutures. Due to crustal thickening during the subduction-related stage, the deeper parts of the overlying metagraywackes and metatonalites contribute melt to the early crustal magma, which eventually solidifies to form monzogranites. Later on, during the post-orogenic stage, anatexis of metapelites can occur, leading to the generation of magmas that give rise to alkali granites.

Keywords: whole-rock geochemistry; late- and post-orogenic granites; Jabal Al Bayda; Hijaz terrain; Arabian Shield



Citation: Abd El-Naby, H.H.; Dawood, Y.H. Geochemical Constraints on the Evolution of Late- to Post-Orogenic Granites in the Arabian Shield, with a Specific Focus on Jabal Al Bayda Area in the Central Hijaz Region, Saudi Arabia. *Appl. Sci.* **2024**, *14*, 735. <https://doi.org/10.3390/app14020735>

Academic Editor: Sotirios Kokkalas

Received: 4 December 2023

Revised: 10 January 2024

Accepted: 12 January 2024

Published: 15 January 2024



Copyright: © 2024 by the authors. Licensee MDPI, Basel, Switzerland. This article is an open access article distributed under the terms and conditions of the Creative Commons Attribution (CC BY) license (<https://creativecommons.org/licenses/by/4.0/>).

1. Introduction

The properties and geochemical signatures of A-type granites contribute to our understanding of the geological history of certain areas, and the tectonic events that have shaped the Earth's crust. The various proposed mechanisms, including fractional crystallization of mafic magma from the mantle (e.g., [1–4]), upwelling of magma from the mantle (e.g., [5,6]), partial melting of lower crustal rocks [7–9], and hybrid origins [10,11] highlight the ongoing debate among researchers about the specific processes involved in the formation of A-type granites. By studying the geochemical behavior of A-type granites, researchers can interpret the sources of magmas, the processes of magma formation and differentiation, and the interactions between mantle and crustal components. This knowledge contributes to a better understanding of the Earth's geological history, the formation of granitic rocks, and the distribution of mineral resources.

The development of the Arabian–Nubian Shield (ANS), a large geological region extending across the Arabian Peninsula and northeastern Africa, has been postulated to have occurred in four main phases [12–16]. During the first stage (~950–850 Ma), oceanic

crust and island arcs were formed. The second stage, which took place from about 850 to 650 Ma, represents the collision and tectonic assembly of different crustal blocks, that led to the formation of the ANS. The post-collision stage 3 of the ANS evolution, occurring approximately between 650 and 580 Ma, is dominated by intermediate to felsic calc-alkaline magmatism. It is also characterized by a transition from compressional to extensional tectonics around 600 Ma. Alkaline to peralkaline granites, andesites, rhyolites, and several episodes of dyke swarms were formed during the fourth stage (~600–530 Ma), which represents late- to post-orogenic intracratonic within-plate magmatism. The specific details regarding the processes involved in generating and emplacing magmas, as well as the timing of transitions between stages are indeed the subject of ongoing scientific debate and research.

During an orogenic cycle, which refers to the formation and evolution of a mountain belt, the composition of magma can change significantly due to various tectonic processes. A notable feature of this cycle is the marked change in the properties of magmatism on a regional scale. Understanding the geodynamic transition between the end of early subduction-related magmatism and the formation of late- to post-orogenic granitic magmas is crucial. To facilitate this understanding and to examine the similarities and differences between the Jabal Al Bayda granitoids and other granitoids of the ANS in terms of their tectonic settings and unique geochemical signatures, we used data from previous studies. The purpose of re-plotting the data is to visually depict the geochemical features of the Jabal Al Bayda granitoids and compare them to other ANS granitoids. In this way, we can identify unique geochemical signatures and recognize the tectonic conditions under which these granitoids were formed. This approach ensures that the present geochemical analysis is relevant and informative as it contributes to the broader research goals of understanding the geodynamic transition and delineating the similarities and differences between the various granitoid suites in the region.

The Jabal Al Bayda area lies within the Arabian Shield (AS), which represents a smaller part of the ANS (Figure 1). The study of the Jabal Al Bayda area can provide valuable insights into the geologic evolution, tectonic processes, and magmatic activity within the AS and, consequently, contribute to our understanding of the broader ANS. In our contribution, we have presented major, trace, and rare earth element compositions of the granitoids of the Jabal Al Bayda area. In combination with published data from similar granitoids in the ANS (Figure 1), the study aims to (1) provide a detailed petrographical and geochemical description of the Jabal Al Bayda granites; (2) constrain the origin of the granitic magma; (3) compare the pre- and post-orogenic granites of the Jabal Al Bayda with alkaline granites of the ANS; and (4) integrate the geochemical data obtained from the studied granites and provide new information on the evolution of the AS.

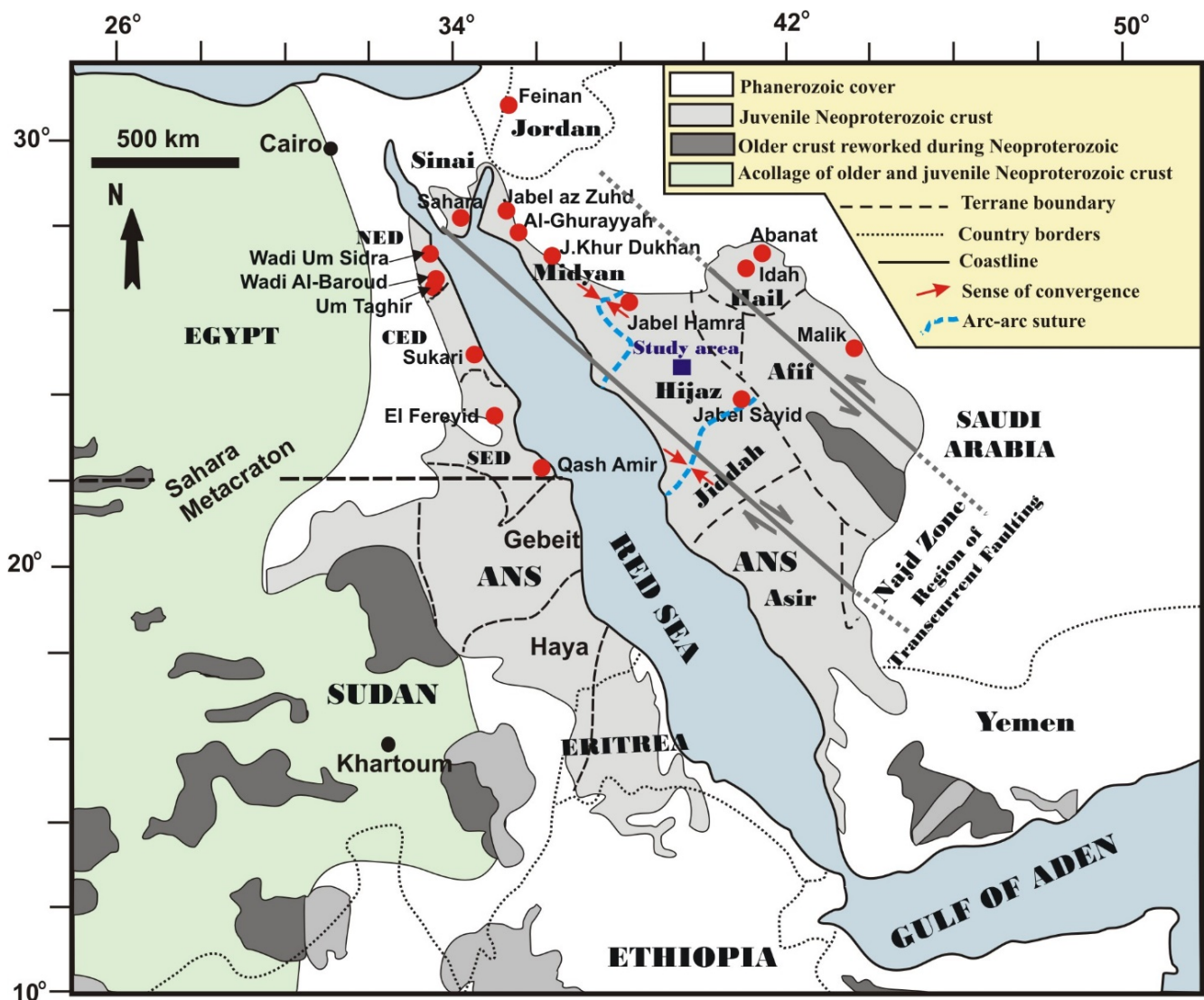


Figure 1. Simplified geological map of the Arabian–Nubian Shield (modified after [17–19]), with the sites of the study area and comparable alkaline granite and monzogranite occurrences in the ANS (red circles). NED, northeastern desert; CED, central-eastern desert; SED, southeastern desert. The Najd Fault System (Najd Zone) and the region of transcurrent faulting is shown (after [20]).

2. General Geology

During the Neoproterozoic, the dominant geological process in the AS was the accretion of island arcs accompanied by several depositional and tectonic cycles [21–23]. Eight distinct accreted tectonostratigraphic terranes have been identified, namely, the western terrains that include Asir (including Jiddah), Hijaz, and Midyan, and the eastern terrains that include Afif and Hail terranes (Figure 1). These terranes are separated by four different suture zones: (1) Yanbu Suture zone that separates the Hijaz and Midyan terranes; (2) Thurwah-Bir Umq Suture zone that separates the Asir and Hijaz terranes; (3) Nabitah Suture zone that separates the Afif terrane from the combined Hijaz-Asir terranes; (4) Al Amar Suture zone that separates the Ar Rayn and Afif terranes.

The classification of granitoids in the AS into three distinct groups was described by [24], providing insights into the geodynamic processes that influenced their formation. The first group is dominated by diorite and trondhjemite, and is characterized by syn-kinematic emplacement between 700 and 900 Ma. The second group is governed by monzogranite and monzonite, and is characterized by late-kinematic emplacement between 620 and 700 Ma. The third group includes intrusives that were emplaced after the major

tectonic activity had ceased (540 to 620 Ma), and are dominantly alkaline to per-alkaline in composition.

3. Geology of the Study Area

The Jabal Al Bayda area is located within Al Madinah quadrangle which is covered by Harrat Rahat basalt for about 75% of its outcrops. The other 25% is made up of Precambrian basement rocks occupying the west edge and the northeast corner of the quadrangle, and are represented by distinct units [25]. Three types of rocks have been identified: Precambrian rocks (Al Ays Group and Furayh Group), plutonic rocks, and Tertiary-Quaternary volcanics (Figure 2). Proterozoic rocks are divided into two groups, namely, the Al Ays Group and the Furayh Group. The Al Ays Group is dominated by old volcanic rocks (700–745 Ma; [26]) that include andesite, dacite, trachyte, rhyolite, and derivative epiclastic and detrital sedimentary rocks. The Al Ays Group includes two main formations: the Farshah Formation comprises several thousand meters thickness of andesite and pyroclastic rock, and the Urayfi Formation consists of felsic volcanic rocks intercalated with volcanic tuff, rhyolite, and transported sedimentary rocks. The Furayh Group (630–660 Ma; [27]) unconformably overlies the Al Ays Group, and its lower part, named Qidirah Formation, consists of mafic volcanic rocks that include andesite, basalt, volcanic breccia, and volcanic tuff (Figure 2). The upper part, named Dawnak Formation, consists of sandstone with conglomerate and thin layers of fine-grained greywacke and siltstone. The granitic rocks outcrop extensively in the Jabal Al Bayda area (Figure 2) and are intersected by a group of felsic and mafic dykes (Figure 3a).

Alkali granites are represented by the granitic outcrops of Jabal Al Bayda. Field observations of these granites imply a relatively homogeneous composition and display pinkish to light gray color and medium-to coarse-grained crystals. Recent petrological and geochemical studies of the Jabal Al Bayda granites indicate that they exhibit post-orogenic A-type geochemical characteristics, and have likely formed in within-plate related tectonic settings [28,29].

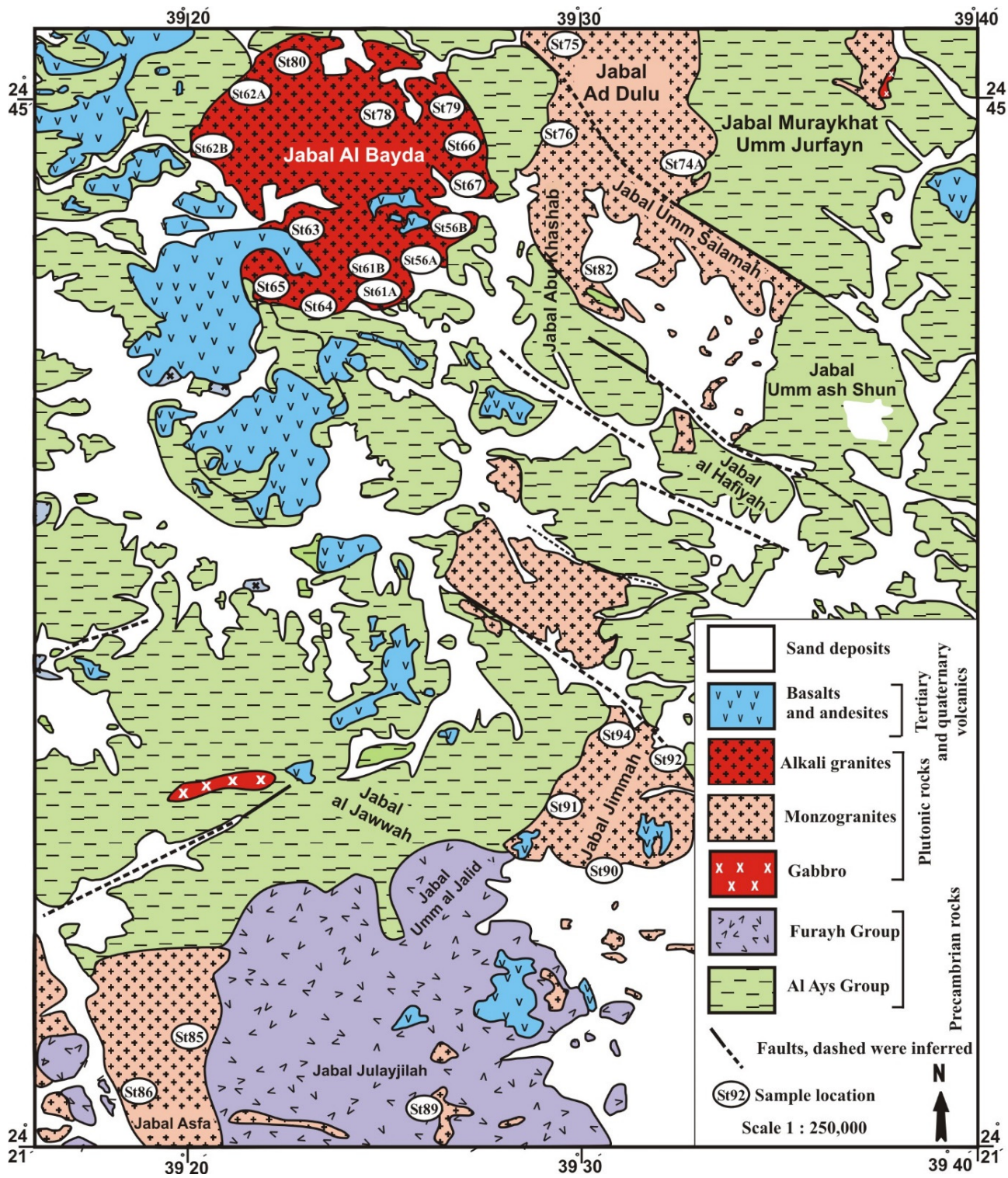


Figure 2. Geological map of the Jabal Al Bayda area (Modified after [28]).

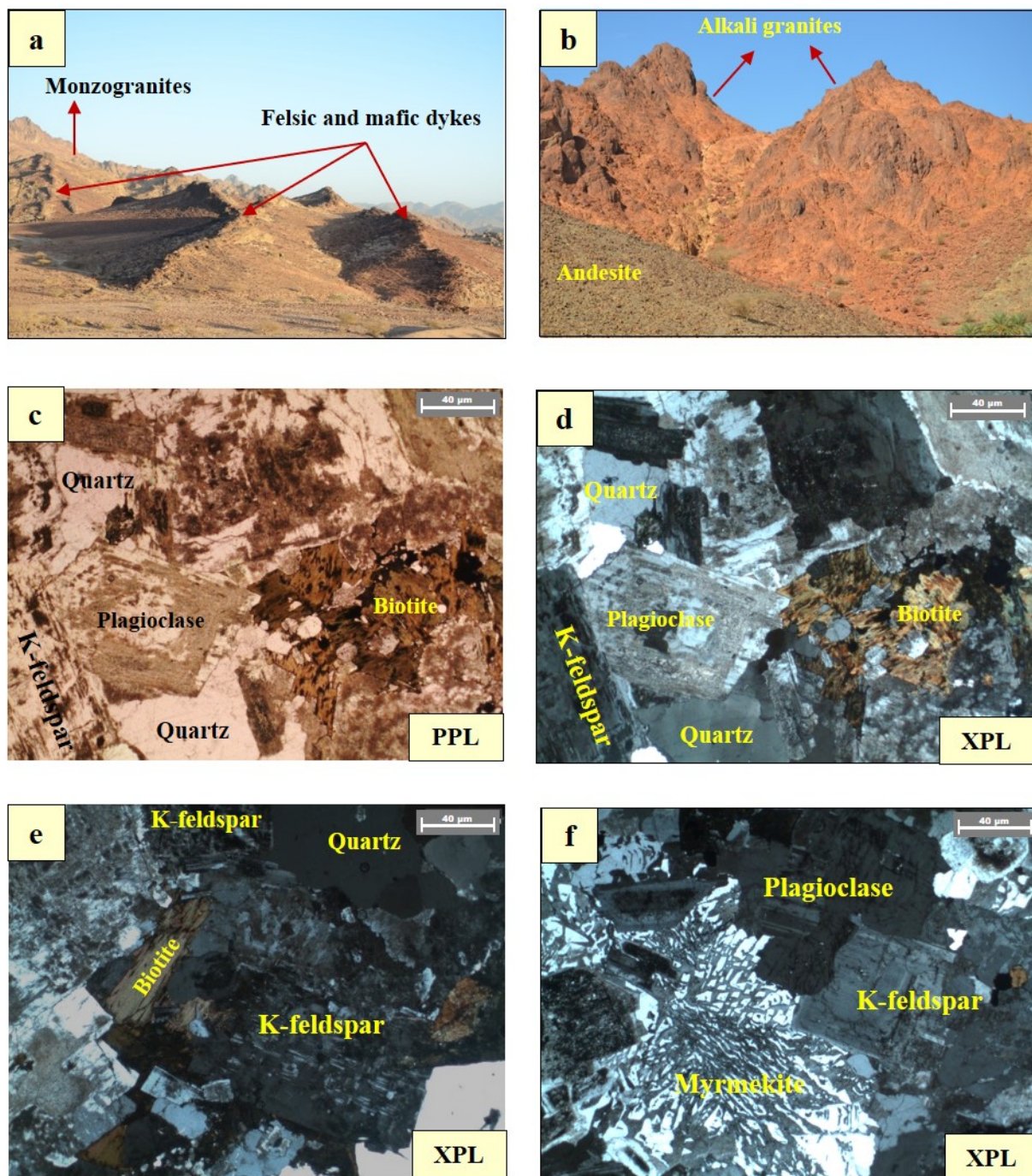


Figure 3. (a) A swarm of felsic and mafic dykes cutting through the monzogranites under investigation. (b) The contact between the studied alkali granites and andesitic rocks of the Al Ays Group. (c,d) Photomicrographs of the monzogranites of Jabal Al Bayda show zoned plagioclase between quartz, K-feldspar, and biotite. (e,f) Photomicrographs showing major minerals of the alkali granite with myrmekitic texture along the quartz-alkali-feldspar contact.

4. Petrographic Characteristics

Based on petrographical analysis, the Jabal Al Bayda pluton is subdivided into monzogranites and alkali granites (Figure 3a,b). Monzogranites are represented by the Jabal Ad Dulu in the northeastern part, the Jabal Jimmah in the central part, and the Jabal Asfa in the southwestern part of the study area (Figure 2). These rocks are megascopically medium- to coarse-grained and have a porphyritic texture. Plagioclase is the dominant mineral in the rock (35–40% by volume), forming sub-euhedral to euhedral crystals and shows zoning

(Figure 3c,d). In places, plagioclase may have undergone alteration, resulting in the formation of epidote and sericite. Quartz is the second dominant mineral, comprising approximately 25–30% of the rock's volume. K-feldspar (20–25% by volume), specifically microcline, is medium-to-coarse-grained and commonly displays Carlsbad twinning. Biotite is present in the rock as euhedral flakes and elongated aggregates. Myrmekitic intergrowths are a distinctive texture observed in this monzogranite. Zircon, magnetite, monazite, and rare titanite and apatite are present as accessory minerals.

Petrographically, alkali granites are dominated by K-feldspars, which make up approximately 55–60% of the rock's composition. Orthoclase appears as subhedral to anhedral tabular crystals. Microcline and microcline-perthite are also present in the alkali granites (Figure 3e), contributing to the overall K-feldspar content. They occur as subhedral crystals showing cross-hatch twinning. Alkali granites contain quartz, comprising about 25–30% of the rock's composition. Plagioclase (oligoclase) is present as compositionally zoned prismatic crystals, constituting approximately 8–11% of the rock's composition. Biotite is present in minor amounts as small irregular flakes, representing less than 2% of the rock's composition. Sub-solidus myrmekite, anti-perthite, and graphic textures are seen (Figure 3f). Accessory minerals are represented by zircon, sphene, and iron oxides, while epidote, sericite, chlorite, and kaolinite are the main secondary minerals.

5. Geochemistry

5.1. Analytical Techniques

Fifty samples were collected from various locations within the Jabal Al Bayda area, representing the spatial variability of the granitic rocks. These samples were prepared for petrographic examination in the "Laboratory for Rock and Thin Section Preparation" at King Abdulaziz University. Once a small piece of a rock sample (2–3 cm in length) has been glued to a slide, it can be further cut, ground, and polished to achieve the desired thickness (typically around 30 microns), which can then be examined under a petrographic microscope. Based on the petrographic observations, 25 samples were selected for subsequent whole-rock geochemical analysis. We focused on the analysis of granitic rocks that had undergone only minimal changes in their chemical composition and mineralogy, i.e., samples that showed little or no replacement of the original minerals by secondary minerals due to alteration processes such as argillization or other hydrothermal changes.

The selected samples were sent to the laboratories of ACME Analytical Laboratories in Vancouver, Canada, for geochemical analysis. The major element analysis was performed using X-ray fluorescence (XRF), with an accuracy of ± 0.01 wt%. In addition, the number of volatiles in the form of loss on ignition (LOI) was measured with an accuracy of 0.01%. Trace and rare earth elements (REE) were measured using the induced coupled plasma mass spectrometer (ICP-MS) method, with an accuracy of 0.01 ppm to 1 ppm. The obtained geochemical data are presented in Tables 1 and 2.

Table 1. Major (wt%), trace (ppm), and rare earth elements (ppm) of selected alkali granites from the Jabal Al Bayda of Central Hijaz Region, Saudi Arabia.

Sample	ST-56A	ST-56B	ST-61A	ST-61B	ST-62A	ST-62B	ST-63	ST-64	ST-65	ST-66	ST-67	ST-78	ST-79	ST-80
SiO ₂	75.07	74.78	76.57	75.37	76.67	75.37	74.87	77.17	79.96	74.28	72.88	76.17	76.27	77.57
TiO ₂	0.16	0.11	0.08	0.11	0.12	0.09	0.15	0.11	0.13	0.15	0.06	0.14	0.11	0.10
Al ₂ O ₃	11.84	11.24	11.48	11.97	11.34	12.01	12.20	11.30	10.19	12.24	12.24	11.56	12.12	10.99
Fe ₂ O ₃	2.50	3.35	1.87	1.82	2.18	1.93	2.16	1.64	1.06	2.32	1.62	1.44	0.92	1.93
MnO	0.01	0.05	0.03	0.02	0.02	0.03	0.04	0.02	<0.01	0.04	0.04	0.04	0.02	0.04
MgO	0.05	0.08	0.04	0.10	0.04	0.08	0.25	0.04	0.03	0.20	0.13	0.07	0.10	0.03
CaO	0.18	0.43	0.35	0.53	0.30	0.26	0.85	0.31	0.18	0.69	1.86	0.56	0.33	0.52
Na ₂ O	3.64	4.22	4.03	4.11	3.81	4.19	4.05	3.71	3.27	4.07	3.36	4.00	3.84	3.66
K ₂ O	5.06	4.27	4.61	4.60	4.44	4.65	4.25	4.74	4.26	4.74	5.24	4.28	4.61	4.59
P ₂ O ₅	<0.01	<0.01	<0.01	0.02	<0.01	0.01	0.03	<0.01	<0.01	0.02	<0.01	<0.01	<0.01	<0.01
Cr ₂ O ₃	0.03	0.03	0.01	0.01	0.02	0.02	0.02	0.01	0.02	0.02	0.01	0.01	0.01	0.01
LOI	0.47	0.57	0.39	0.65	0.52	0.38	0.42	0.44	0.49	0.46	1.97	0.85	0.81	0.43
Sum	99.02	99.12	99.46	99.31	99.45	99.02	99.28	99.48	99.58	99.22	99.42	99.11	99.13	99.87
La	110.27	23.13	44.37	59.42	41.28	38.88	40.98	58.62	62.61	62.91	16.95	59.62	164.41	58.03
Ce	207.48	48.95	95.81	116.15	98.40	80.86	88.13	121.04	137.29	132.20	35.49	124.13	94.91	127.22
Pr	25.58	6.05	12.16	12.66	12.19	11.22	10.59	14.34	16.50	15.34	4.52	16.32	34.58	14.87

Table 1. Cont.

Sample	ST-56A	ST-56B	ST-61A	ST-61B	ST-62A	ST-62B	ST-63	ST-64	ST-65	ST-66	ST-67	ST-78	ST-79	ST-80
Nd	89.23	20.24	43.27	43.27	43.97	36.89	36.29	47.66	58.62	55.43	16.45	52.64	131.70	48.45
Sm	17.53	5.79	11.10	10.49	11.70	11.09	8.58	10.13	12.47	12.53	4.70	15.57	32.85	11.10
Eu	0.24	0.10	0.09	0.18	0.13	0.12	0.40	0.12	0.11	0.26	0.17	0.15	0.49	0.11
Gd	15.63	6.17	10.90	10.45	11.92	11.03	8.34	9.16	10.38	11.78	5.08	14.78	37.27	9.89
Tb	2.36	1.19	1.84	1.91	2.10	2.00	1.52	1.44	1.67	1.99	0.99	2.68	4.55	1.65
Dy	12.36	7.09	10.69	11.46	12.16	12.20	9.50	8.38	9.76	12.64	5.91	16.48	20.19	10.15
Ho	2.42	1.64	2.25	2.49	2.53	2.44	1.86	1.62	1.98	2.52	1.26	3.47	3.49	1.96
Er	7.03	5.13	6.19	6.99	7.59	6.93	5.53	4.86	5.57	7.11	4.06	9.60	8.38	6.16
Tm	1.10	0.87	1.04	1.13	1.10	1.10	0.92	0.69	0.89	1.18	0.66	1.52	1.20	0.99
Yb	7.18	5.66	5.97	7.30	6.71	5.97	5.64	5.07	6.04	7.30	4.57	9.68	7.13	6.30
Lu	1.21	0.98	0.92	1.13	1.09	0.99	0.96	0.77	1.03	1.14	0.69	1.53	1.18	1.06
Y	75.47	46.66	66.00	67.90	73.58	67.50	58.62	49.15	56.83	80.16	39.38	97.81	97.71	55.33
Hf	15.15	8.47	9.17	14.56	12.66	11.47	9.67	9.37	12.66	12.46	4.49	15.15	9.77	10.97
Nb	44.47	48.25	37.29	59.02	45.96	43.97	42.67	33.10	49.45	57.23	24.03	58.92	49.55	43.37
Ta	3.09	3.79	2.39	4.59	2.79	2.79	3.79	2.19	4.09	4.59	2.69	4.39	3.69	2.59
Th	21.63	11.96	12.36	18.05	15.35	15.35	19.14	14.06	17.95	23.83	23.93	21.83	19.04	15.55
Zn	41.87	92.72	88.73	85.74	69.79	61.81	54.84	43.87	11.96	64.81	28.91	47.86	11.96	59.82
Co	1.30	1.00	0.60	1.30	0.80	0.90	1.99	0.70	0.20	1.69	1.60	0.90	0.80	2.39
Ni	5.18	2.89	1.99	2.19	3.99	2.69	4.59	1.79	2.19	2.69	2.69	1.69	1.89	1.60
Ba	50.85	39.88	9.97	108.67	61.81	84.75	253.2	24.93	9.97	140.5	208.3	62.81	109.6	12.96
V	12.96	10.97	10.97	12.96	9.97	7.98	14.96	<8	<8	9.97	10.97	<8	<8	<8
Cu	3.69	6.68	1.89	2.69	3.49	4.79	1.99	3.89	2.79	3.39	2.09	1.50	2.79	1.30
Sr	12.66	10.97	7.68	40.88	31.60	25.12	87.24	15.15	6.98	46.26	80.26	29.41	44.17	5.98
Zr	528.51	257.43	275.87	359.52	370.58	308.37	261.31	322.83	363.61	357.32	92.12	390.43	253.04	307.67
Rb	168.39	183.85	172.98	189.13	148.85	179.76	190.93	150.95	152.84	226.82	191.82	192.22	183.65	155.43
As	1.00	1.20	2.19	1.00	0.60	1.50	1.30	1.69	2.19	1.60	<0.5	5.88	<0.5	6.48
Be	3.99	11.96	3.99	8.97	3.99	1.99	4.99	3.99	2.99	4.99	9.97	2.99	15.95	7.98
Sb	0.10	0.10	0.20	0.10	0.10	0.20	0.20	0.10	0.10	0.20	<0.1	0.20	<0.1	0.20
Sn	7.98	12.96	6.98	6.98	6.98	5.98	4.99	6.98	9.97	7.98	3.99	13.96	4.99	8.97
U	5.18	5.48	5.18	7.28	6.08	6.38	8.28	4.89	5.98	7.58	11.07	9.67	4.09	5.38
W	2.19	<0.5	0.50	1.60	1.50	1.60	1.69	2.39	1.60	1.00	<0.5	3.29	0.80	1.89
Cd	<0.1	0.10	<0.1	<0.1	<0.1	<0.1	<0.1	<0.1	<0.1	<0.1	<0.1	<0.1	<0.1	<0.1
Cs	1.10	0.90	1.89	1.69	1.20	1.69	1.99	2.09	2.19	4.19	0.90	3.09	1.10	1.60
Ga	23.33	31.21	24.63	26.22	24.23	24.33	22.13	23.13	21.83	25.62	19.84	25.92	24.93	22.23
Mo	5.58	2.89	2.19	2.79	2.89	2.69	2.49	2.49	1.69	2.89	1.79	2.99	1.00	4.69
Pb	11.86	15.85	8.18	5.28	10.77	7.88	12.16	9.27	6.38	9.07	15.45	8.47	4.09	9.67
Ag	<0.1	<0.1	<0.1	<0.1	<0.1	<0.1	<0.1	<0.1	<0.1	<0.1	<0.1	<0.1	<0.1	<0.1
Au	2.69	<0.5	<0.5	<0.5	<0.5	<0.5	<0.5	0.80	0.70	1.40	<0.5	1.50	<0.5	<0.5
Eu/Eu*	0.044	0.051	0.025	0.052	0.034	0.033	0.144	0.038	0.029	0.065	0.106	0.030	0.043	0.032
Y/Nb	1.70	0.97	1.77	1.15	1.60	1.54	1.37	1.48	1.15	1.40	1.64	1.66	1.97	1.28
Rb/Sr	13.30	16.76	22.53	4.63	4.71	7.15	2.19	9.96	21.90	4.90	2.39	6.54	4.16	25.98
Nb/Ta	14.39	12.74	15.58	12.87	16.46	15.75	11.26	15.09	12.10	12.48	8.93	13.43	13.43	16.73

Table 2. Major (wt%), trace (ppm), and rare earth elements (ppm) of selected monzogranites from the Jabal Al Bayda of Central Hijaz Region, Saudi Arabia.

Sample	ST-74A	ST-75	ST-76	ST-82	ST-85	ST-86	ST-89	ST-90	ST-91	ST-92	ST-94
SiO ₂	65.10	65.40	68.79	68.59	71.58	71.29	68.00	69.39	69.49	69.39	66.80
TiO ₂	0.57	0.51	0.53	0.50	0.26	0.29	0.54	0.39	0.36	0.34	0.39
Al ₂ O ₃	16.43	16.85	14.66	14.52	14.21	14.66	14.55	14.31	14.60	14.63	14.16
Fe ₂ O ₃	3.19	2.59	2.85	3.07	1.76	2.05	3.44	2.87	2.78	2.72	2.48
MnO	0.05	0.06	0.04	0.06	0.03	0.03	0.05	0.08	0.06	0.06	0.05
MgO	1.24	0.69	1.14	1.22	0.43	0.52	1.19	0.53	0.48	0.45	0.37
CaO	2.41	1.85	2.22	2.27	1.12	1.70	2.40	1.08	1.35	1.03	2.70
Na ₂ O	5.08	5.53	4.57	4.35	4.28	4.15	4.31	4.64	4.77	4.77	4.44
K ₂ O	3.85	4.83	3.70	4.02	4.51	3.86	3.80	4.75	4.69	4.75	4.40
P ₂ O ₅	0.19	0.12	0.16	0.18	0.07	0.10	0.12	0.09	0.09	0.07	0.08
Cr ₂ O ₃	0.02	0.01	0.01	0.01	0.01	0.02	0.02	0.01	0.02	0.02	0.01
LOI	1.48	0.81	0.67	0.40	0.88	0.58	0.89	1.10	0.53	0.93	3.22
Sum	99.61	99.25	99.33	99.18	99.14	99.24	99.29	99.22	99.20	99.14	99.09
La	32.50	41.77	30.11	30.51	31.01	24.13	19.94	42.07	33.10	38.48	36.39
Ce	64.61	97.21	58.62	63.01	59.02	49.75	44.77	88.73	73.78	80.46	78.76
Pr	7.41	11.92	6.60	7.51	6.61	5.37	5.37	10.41	8.42	9.01	9.10
Nd	25.32	36.99	22.23	26.42	22.63	16.65	19.94	37.49	29.51	32.60	36.19
Sm	4.37	6.50	3.90	4.78	3.80	2.69	4.12	6.97	5.89	5.53	6.43
Eu	1.31	1.37	1.04	1.10	0.83	0.78	1.01	0.91	0.80	0.79	0.83
Gd	3.18	4.69	2.70	3.50	2.70	1.78	3.67	6.30	5.28	5.23	6.12
Tb	0.44	0.66	0.35	0.50	0.32	0.19	0.59	1.06	1.02	0.97	1.05
Dy	2.06	3.31	1.81	2.44	1.73	0.82	3.43	6.45	6.37	5.41	6.16
Ho	0.42	0.62	0.32	0.49	0.30	0.17	0.74	1.37	1.37	1.14	1.46

Table 2. Cont.

Sample	ST-74A	ST-75	ST-76	ST-82	ST-85	ST-86	ST-89	ST-90	ST-91	ST-92	ST-94
Er	1.16	1.82	0.72	1.52	0.70	0.42	2.09	4.15	4.16	3.40	4.10
Tm	0.15	0.25	0.12	0.24	0.11	0.05	0.32	0.65	0.69	0.57	0.65
Yb	1.05	1.63	0.72	1.39	0.70	0.38	2.21	4.69	4.54	3.69	4.27
Lu	0.15	0.24	0.14	0.24	0.09	0.06	0.38	0.75	0.73	0.58	0.66
Y	10.77	17.65	9.37	15.05	8.97	4.39	20.94	39.98	38.68	33.80	40.48
Hf	5.38	7.38	4.69	5.28	4.39	4.79	5.28	10.17	8.87	8.67	9.07
Nb	8.97	10.37	8.18	9.07	12.26	7.28	5.98	9.27	9.77	9.47	8.57
Ta	0.60	0.80	0.70	0.70	0.80	0.40	0.50	0.80	0.90	0.60	0.80
Th	7.58	6.08	8.77	9.67	11.86	7.58	6.88	12.66	10.87	11.07	9.87
Zn	42.87	39.88	26.92	30.91	36.89	37.89	22.93	55.83	27.92	42.87	27.92
Co	6.68	3.19	7.28	6.48	2.59	3.39	7.18	3.19	3.39	3.09	3.09
Ni	11.57	2.29	9.67	8.57	2.69	3.89	10.17	3.29	3.99	3.59	3.29
Ba	1154.53	1409.76	746.75	968.09	823.52	925.22	532.40	372.88	342.97	370.88	330.01
V	47.86	32.90	43.87	42.87	19.94	20.94	42.87	18.94	23.93	23.93	21.93
Cu	6.58	4.09	2.29	2.19	3.99	5.88	7.38	4.59	25.72	6.98	3.59
Sr	837.68	521.03	650.34	674.17	328.41	369.39	259.52	130.01	125.42	132.00	101.20
Zr	200.80	312.46	172.18	178.16	159.82	159.12	213.56	352.44	317.54	302.89	328.71
Rb	68.29	61.12	88.73	94.81	134.50	105.08	98.60	143.07	129.91	127.62	114.36
As	0.90	1.00	1.20	0.50	0.60	1.20	1.10	7.68	<0.5	<0.5	<0.5
Be	<1	<1	1.99	3.99	1.00	1.99	1.00	1.99	3.99	8.97	7.98
Sb	<0.1	<0.1	<0.1	<0.1	<0.1	<0.1	0.20	0.50	0.60	0.70	0.10
Sn	<1	1.00	<1	<1	<1	<1	1.99	2.99	4.99	3.99	2.99
U	2.59	1.99	2.59	4.89	2.69	1.60	2.59	4.69	5.08	3.89	2.89
W	<0.5	<0.5	<0.5	<0.5	1.90	<0.5	<0.5	1.00	<0.5	<0.5	<0.5
Cd	<0.1	<0.1	<0.1	<0.1	<0.1	<0.1	<0.1	<0.1	<0.1	<0.1	0.10
Cs	1.00	1.20	1.69	3.29	1.20	1.69	1.40	1.79	3.99	1.99	1.40
Ga	19.84	18.84	19.74	17.35	19.54	19.64	17.55	19.74	18.84	18.44	18.25
Mo	0.80	0.80	1.10	1.30	0.60	0.90	1.20	2.09	2.39	2.69	1.99
Pb	4.49	3.59	3.49	2.59	5.48	3.59	5.48	16.45	9.67	16.65	11.07
Ag	<0.1	<0.1	<0.1	<0.1	<0.1	<0.1	<0.1	<0.1	<0.1	<0.1	<0.1
Au	<0.5	<0.5	0.60	<0.5	6.78	<0.5	1.50	1.40	14.46	11.66	8.67
Eu/Eu*	1.071	0.756	0.976	0.820	0.789	1.084	0.792	0.418	0.437	0.447	0.403
Y/Nb	1.20	1.70	1.15	1.66	0.73	0.60	3.50	4.31	3.96	3.57	4.72
Rb/Sr	0.08	0.12	0.14	0.14	0.41	0.28	0.38	1.10	1.04	0.97	1.13
Nb/Ta	15.00	13.00	11.71	13.00	15.38	18.25	12.00	11.63	10.89	15.83	10.75

5.2. Bulk-Rock Geochemistry

The granites examined can be classified using the R1–R2 cationic classification of [30], with the monzogranite samples being assigned to the monzogranite field, with the exception of two samples that are assigned to the quartz-monzonite and quartz-syenite fields (Figure 4). The majority of the alkali granites from the Jabal Al Bayda are plotted within the alkali-feldspar granite field, with one sample that straddles the boundary between alkali-feldspar granite and monzogranite fields, and another one that falls in the monzogranite field (Figure 4).

The granitic samples from the study area exhibit a range of silica (SiO₂) content, the low-silica monzogranite (65.10–71.58 SiO₂ wt%), and high-silica alkali granite that contains 72.88–79.96 SiO₂ wt%. Based on Figure 5, it is observed that the selected major and trace elements exhibit medium to weak correlations with silica (SiO₂) variance in the granite samples. However, there is a definite clustering for different granitic types into two distinct fields. Na₂O, Al₂O₃, TiO₂, P₂O₅, CaO, MgO, Fe₂O₃, Co, V, Ba, Ni, and Sr contents show negative correlations with SiO₂ contents. The values of these elements are remarkably higher in monzogranites compared to alkali granites. Similarly, Ta contents display a negative correlation with silica (SiO₂), while Nb and Sn contents show a positive correlation with SiO₂. The values of these elements are higher in alkali granites (Figure 5). The differences in magmatic trends observed for K₂O, Rb, Y, Hf, Th, and U contents among

the different granitic types in the Jabal Al Bayda area suggest that a simple fractional crystallization model is inadequate to explain the origin of the granitoids in this region.

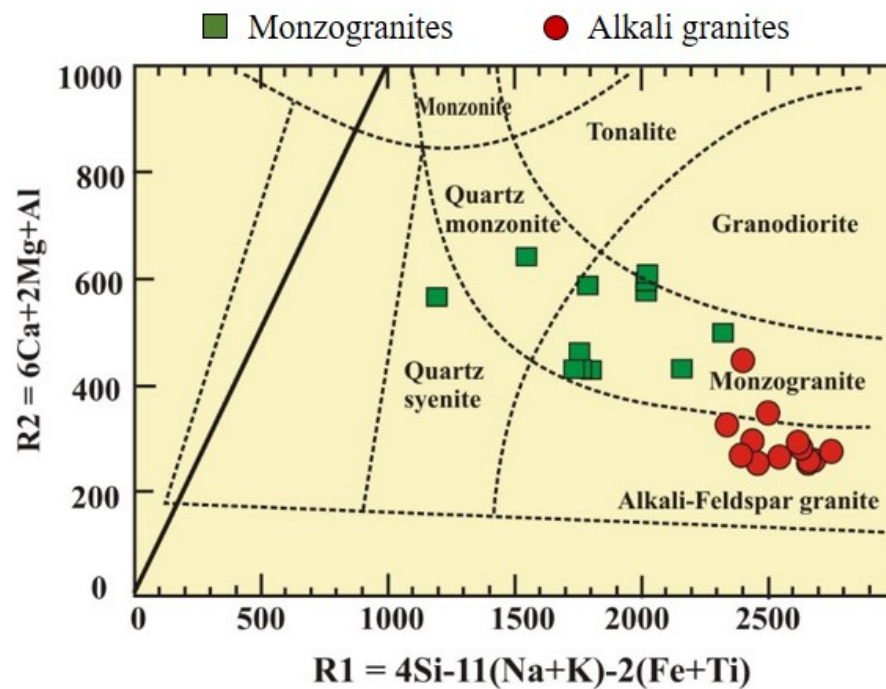


Figure 4. Classification of the studied granitic samples according to the R1–R2 diagram [30].

In the classification based on the ACNK versus ANK diagram [31], the monzogranites from the Jabal Al Bayda are classified as metaluminous to weakly peraluminous (Figure 6a). Conversely, alkali granites straddle the boundary between metaluminous and peralkaline fields. Similarly to the alkaline granites and monzogranites from the ANS, the studied granitoids are characterized by an enrichment in alkalis ($\text{Na}_2\text{O} + \text{K}_2\text{O} = 7.53\text{--}10.36$ wt%). Furthermore, the data suggest that all the samples are plotted within the alkaline field (Figure 6b). In the K_2O vs. SiO_2 diagram (Figure 6c), these samples are plotted within the field of the shoshonite series. Monzogranites, on the other hand, typically exhibit $\text{K}_2\text{O}/\text{Na}_2\text{O}$ ratios less than 1, which aligns with their high-K calc-alkaline nature. However, it is also important to mention that some samples within the monzogranite group are plotted within the shoshonite series. The studied alkali granites and monzogranites are plotted within the ferroan field in the $\text{FeO}_t/(\text{FeO}_t + \text{MgO})$ versus SiO_2 diagram (Figure 6d). However, a few monzogranite samples are plotted in the magnesian field. The ferroan nature of the studied granitoids is similar to the most of rare-metal granites in the ANS. It is also important to note that there are exceptions within the ANS, where certain intrusions display a magnesian nature, e.g., alkali feldspar granite from the Um Taghir area, Egypt [32] and monzogranite from the El Fereyid area, Egypt [33].

The chondrite normalized REE patterns of the alkali granites and monzogranites are quite different (Figure 7a,b). The REE contents of alkali granites are higher than those of the monzogranites. The two patterns demonstrate fractionation in LREEs and flat HREEs (Figure 7a,b). The alkali granites display a strong negative Eu anomaly ($\text{Eu}/\text{Eu}^* = 0.025\text{--}0.144$, with an average of 0.052), and show similar chondrite-normalizing REE patterns of the ANS alkali-feldspar granites. Conversely, the monzogranites show a low Eu anomaly (average $\text{Eu}/\text{Eu}^* = 0.73$).

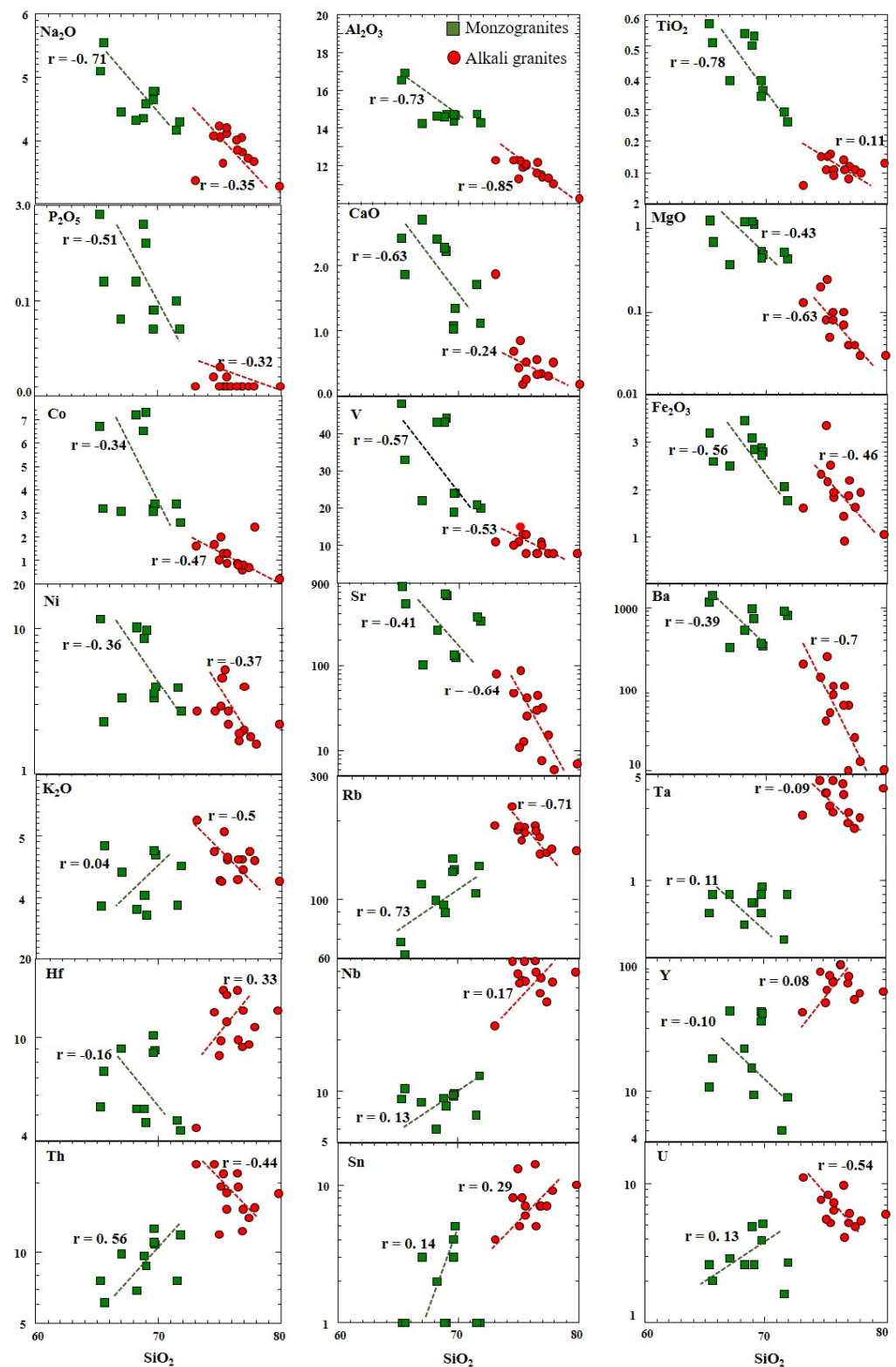


Figure 5. Harker variation diagrams, showing negative correlations of Na₂O, Al₂O₃, TiO₂, P₂O₅, CaO, MgO, Fe₂O₃, Co, V, Ba, Ni, Sr, and Ta with SiO₂, whereas Nb and Sn show positive correlations. K₂O, Rb, Y, Hf, Th, and U show different magmatic trends for each rock type.

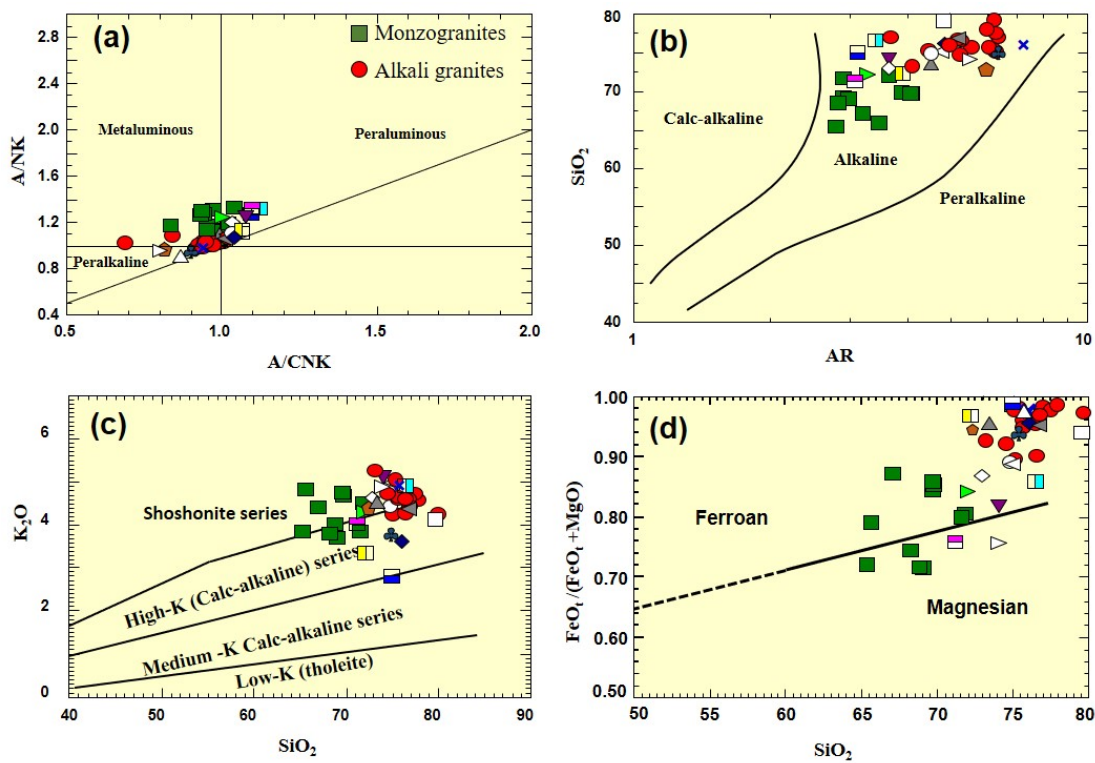


Figure 6. Magma type diagrams of the Jabal Al Bayda granites; (a) A/CNK vs. A/NK diagram [31], (b) AR vs. SiO₂ diagram [34], AR (Alkalinity Ratio) = $[\text{Al}_2\text{O}_3 + \text{CaO} + (\text{Na}_2\text{O} + \text{K}_2\text{O})]/[\text{Al}_2\text{O}_3 + \text{CaO} - (\text{Na}_2\text{O} + \text{K}_2\text{O})]$, (c) K₂O vs. SiO₂ diagram [35], and (d) FeO/(FeO_t + MgO) vs. SiO₂ diagram of [36]. **Alkaline granites from Saudi Arabia:** \triangle : Monzogranite from Abanat area [37]. \diamond : Monzogranite from Jabal Khur Dukhan Complex [38]. \blacklozenge : Alkali feldspar granite from Jabal az Zuhd area [38]. \blacktriangleleft : Alkali feldspar granite from Idah area [37]. \blacktriangledown : Alkali feldspar granite from Malik area [37]. \blacktriangle : Alkali feldspar granite from Al-Hamra area [39]. \blacksquare : Alkali feldspar granite from Al-Ghurayyah area [40]. \clubsuit : Alkali feldspar granite from Jabal Sayid area [40]. **Alkaline granites from Jordan:** \square : Monzogranite from Feinan [41]. **Alkaline granites from Egypt:** \blacksquare : Monzogranite from Sukari area [42]. \blacklozenge : Monzogranite from Um Taghir; \square : Monzogranite from El Fereyid area [33]. \blacksquare : Monzogranite from Wadi Al-Baroud area [43]. \blacktriangleright : Monzogranite from Wadi Um Sidra area. \blacktriangleleft : Alkali feldspar granite from Wadi Um Sidra. \circ : Alkali feldspar granite from Qash Amir area [44]. \blacktriangleright : Alkali feldspar granite from Um Taghir area [32]. \times : (A2) alkaline granites from Sahara area [45].

The normalization of trace element concentrations in the alkali granites to ORG values [4] indicates that the alkali granites have broadly similar patterns to those of ANS alkali-feldspar granites. Both are enriched in K, Rb, Th, Ta, and Nb, and have negative Ba and Zr anomalies (Figure 7c). This indicates that crustal materials contributed significantly to the composition of these granites. Concerning monzogranites, as shown in Figure 7d, two groups of elements are observed in these granites and their comparison with ANS monzogranites. The first group of elements consists of large ion lithophile elements (LILE), including K, Rb, Ba, and Th, which are observed to be enriched relative to the ORG values of [4], and display higher concentrations compared to the corresponding monzogranites of the ANS. The second group of elements includes Zr, Sm, Y, and Yb, which are observed to be less than one in most cases. The observed trace element patterns in the studied monzogranites align with those typically found in ANS monzogranites associated with island/continental arc settings.

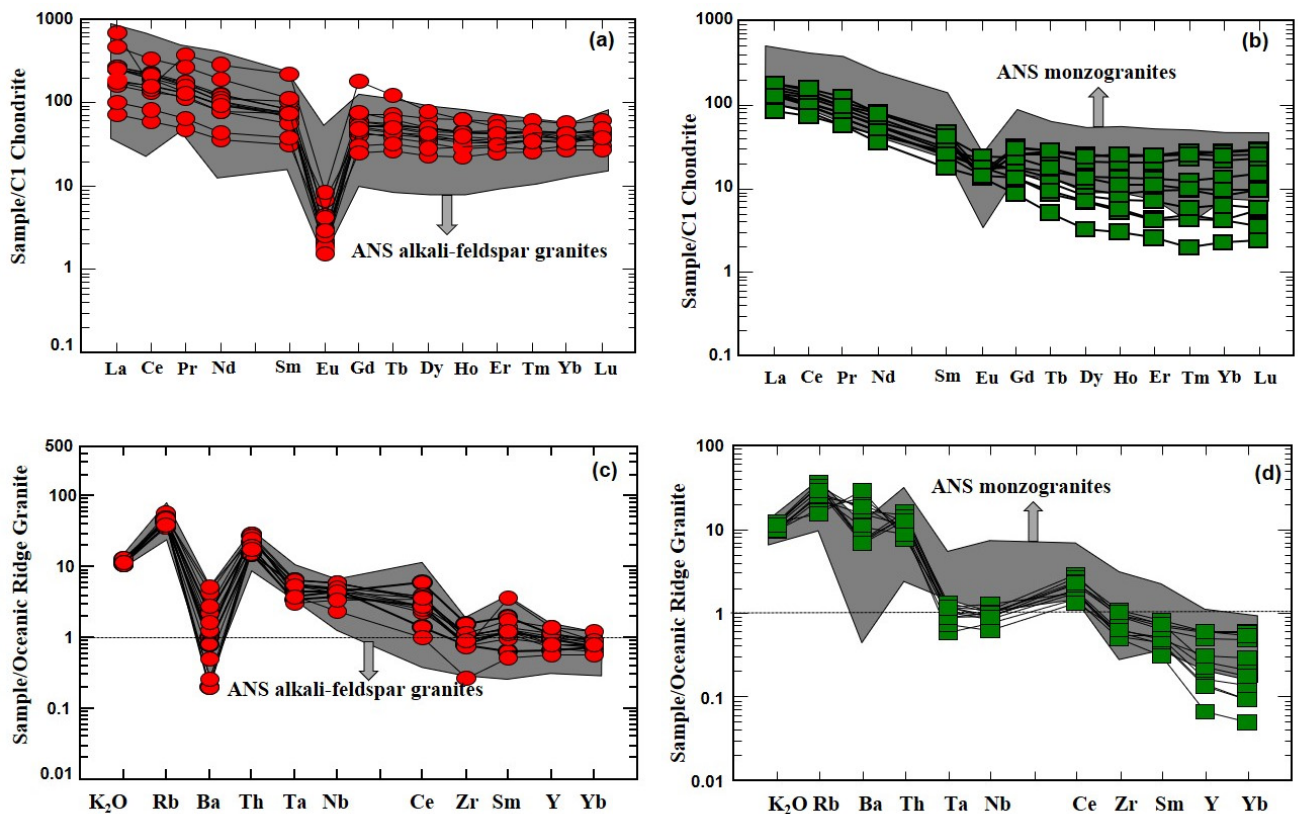


Figure 7. Chondrite-normalized REE patterns [46] for (a) the alkali granites, (b) the monzogranites. The mid-oceanic ridge granite normalized spider diagram of trace elements [4] for (c) the alkali granites and (d) the monzogranites, in comparison with the ANS alkali-feldspar granite and monzogranite patterns of selected areas showed in Figure 1.

6. Discussion

6.1. Tectonic Setting

In the Ta, Hf, and Rb diagram of [47], the Jabel Al Bayda monzogranites are plotted within the volcanic-arc granite (VAG, Figure 8a), similarly to the monzogranites from the Wadi Um Sidra area, Egypt [48]. However, most of the alkali granites samples are plotted in the within-plate granite field (WPG), comparable to the alkaline granites of Saudi Arabia (e.g., Jabal Khur Dukhan, Jabal az Zuhd, Al-Hamra, and Al-Ghurayyah areas), and monzogranite from the Wadi Al-Baroud area, Egypt [43], while only one sample of the alkali granites is plotted within the post-COLG setting, similarly to alkali granites from the Wadi Um Sidra area, Egypt [48].

The Th/Ta ratio vs. Yb diagram helps to outline the tectonic environment of magmatism (Figure 8b). It is suggested that the alkali granites formed in an ensimatic rift setting, comparable to the alkaline granites of Saudi Arabia, e.g., the alkali feldspar granite from the Al-Hamra area [39], Jabal Sayid area [40], Idah area [37], and Jabal az Zuhd area [38]. On the other hand, the monzogranites are regarded as subduction-related arc granitoids at an active continental margin setting, similarly to Egyptian monzogranites from the El Fereyid area [33], Wadi Um Sidra area [48], and Wadi Al-Baroud area [43].

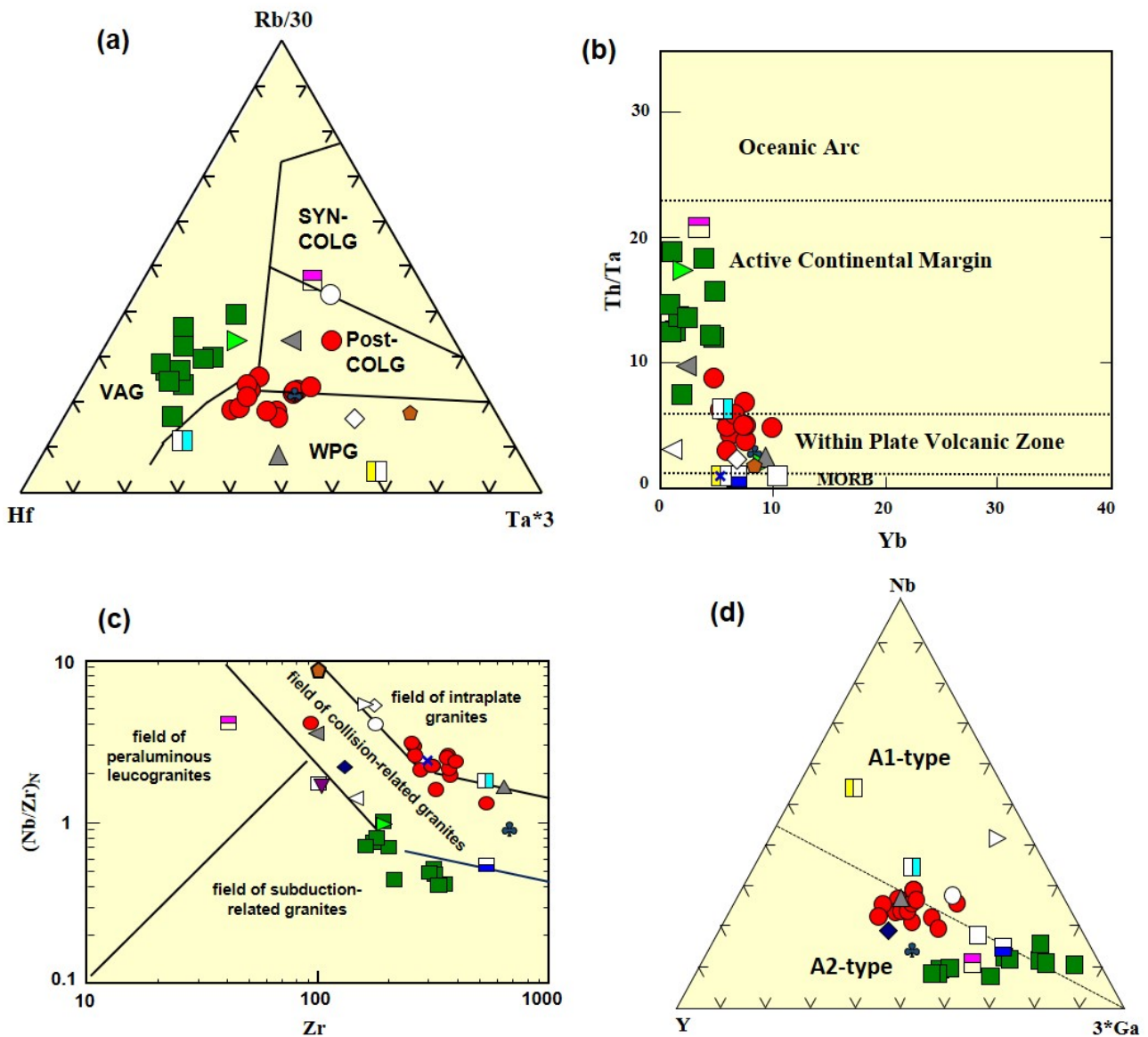


Figure 8. (a) Rb/30-Hf-Ta*3 ternary diagram of [47], for various tectonic environments in collision zones, (b) Th/Ta vs. Yb tectonic discrimination diagram of [49], (c) Zr vs. $(\text{Nb}/\text{Zr})_N$ diagram of [50], normalization values from [46], (d) Nb-Y-Ga*3 ternary diagram of [2]. VAG = volcanic arc granite; SYN-COLG = syn-collision granite; Post-COLG = post-collisional granite; WPG = within-plate granite. Symbols are as indicated in Figure 6.

The Zr vs. $(\text{Nb}/\text{Zr})_N$ diagram enables a clear discrimination between two magmatic series (Figure 8c). The early magmatic series, represented by the Jabal Al Bayda monzogranites, is plotted in the subduction-related field, similarly to the Egyptian monzogranite from the Sukari area [42], Wadi Um Sidra area [48], Um Taghir area [32], and Feinan area, Jordan [41], whereas the late magmatic series of alkali granites falls within the field of intraplate granites, except three samples that belong to the collision-related granites, similarly to the alkali feldspar granites from Saudi Arabia, e.g., the Jabal Sayid area [40], Al-Hamra area [39], and Jabal az Zuhd area [38]; A2 alkaline granites from Sahara area, Sinai [45]; and alkali feldspar granite from Egypt, e.g., the Qash Amir area [44] and Um Taghir area [32]. There are similarities between the studied granitoids and the 559 ± 6 Ma Sukari monzogranite of [51], the 556–572 Ma Feinan Ghuweir Magmatic Suite of [41], the 593 ± 2.4 Ma Jabal Sayid alkali granite of [52], the 564 ± 140 Ma Jabal az Zuhd alkali feldspar granite of [38], and the 608–578 Ma Sahara alkaline granites of [45]. The presence of two magmatic

series may indicate a change in tectonic processes or conditions during the evolution of the magmatic system in the ANS. The observed transition from a subduction-related signature to a collision or intraplate signature from the early to late magmatic series provides valuable insights into the evolving tectonic processes and geodynamic history of the region.

Based on the Nb-Y-3Ga ternary diagram for discrimination of A1- and A2-type granites [2], samples of Al Bayda alkali granites are plotted into A2-type granites (Figure 8d), which is in agreement with the general understanding of the alkaline granites in the ANS, where numerous alkaline granites have been documented to have a crustal origin (e.g., Jabal Sayid and Al-Hamra granites), except one sample that fall in A1-type granite, similarly to the alkali feldspar granite from the Qash Amir area, Egypt [44] and alkali feldspar granite from Um Taghir area [32]. Samples of Al Bayda monzogranites straddle the boundary between A1- and A2-type magmatic suites, similarly to the monzogranite from the Wadi Al-Baroud area [43], Sukari area [42], Feinan area [41], El Fereyid area [33], and the alkali-feldspar granite from Al-Ghurayyah area [40], Qash Amir area [44], and Um Taghir area [32].

Group A1 and Group A2 represent different types of granitoids formed in different tectonic environments. Group A1 granitoids are associated with global continental and oceanic rifting, resulting in horizontal crustal extension and lithospheric plate fracturing. The magmas originate from the melting of the subcontinental lithospheric mantle and lower crust. Group A2 granitoids, on the other hand, form in local expansion zones in intracontinental and continental margin areas. They are the result of the expansion and thinning of the continental crust, with the gaps being filled by upwelling magmas originating from the mantle [53]. The Jabal Al Bayda A2 monzogranites, typically derived from subduction-related processes (Figure 8c), may interact with the crustal rocks in the collision zone. This interaction can lead to mixing of magmas and crustal material, resulting in the formation of granites with anorogenic properties. The Y/Nb ratio is a geochemical parameter used to evaluate the association of granitic rocks with crustal processes. A Y/Nb ratio above 1.2 is often considered to indicate an influence of the crust on granite formation. In the case of the Jabal Al Bayda granites, as mentioned in Tables 1 and 2, the Y/Nb ratio indicates an association with crustal processes.

6.2. Petrogenesis of the Jabal Al Bayda Granitic Magma

Several models have been postulated to explain the petrogenesis of the granitic rocks in the ANS. These alternative models include (1) the fractional crystallization model, as proposed by [54–57], and other researchers, which suggests that the granitic rocks in the ANS formed through the process of fractional crystallization of mantle-derived magmas; (2) the magma mixing model, as suggested by [58], which proposes that the granitic rocks in the ANS formed through mixing of felsic and mafic magmas; and (3) the partial melting model, as proposed by [59–64], and others, which suggests that the granitic rocks in the ANS formed through partial melting of either an ancient, enriched lithospheric mantle or a relatively young and less evolved crust. By examining the geochemical characteristics of the Jabal Al Bayda granitic rocks, it would be possible to assess which of these alternative mechanisms best explains their petrogenesis.

The high silica contents (average of SiO₂ is 68 wt% and 76 wt% for monzogranites and alkali granites, respectively) and enriched and fractionated LREE patterns observed in the Jabal Al Bayda monzogranites and alkali granites are inconsistent with a model of fractional crystallization of mantle materials. The Rb/Sr ratio is a geochemical indicator that can be used to distinguish between mantle-derived magmas and those derived from continental crust. Mantle-derived magmas typically have very low Rb/Sr ratios (Rb/Sr < 0.1; [65]), while continental crustal rocks tend to have higher Rb/Sr ratios [66]. In the case of the Jabal Al Bayda granitic rocks, the average Rb/Sr ratios of 0.53 for the monzogranites and 10.51 for the alkali granites, as reported in Tables 1 and 2, are higher than the Rb/Sr ratios expected for mantle-derived magmas. These elevated Rb/Sr ratios are more consistent with a continental crustal source rather than a mantle source (Figure 9a).

The Nb/Ta ratios and Y/Nb ratios further support the model of the Jabal Al Bayda granitic rocks originating from the partial melting of a relatively juvenile crust. Mantle-derived rocks typically exhibit higher Nb/Ta ratios (>17.5), whereas continental crustal materials have lower Nb/Ta ratios (<17.5) [66,67]. In the case of the Jabal Al Bayda granitic rocks, the average Nb/Ta ratios of 13.40 for monzogranites and 13.66 for alkali granites, as reported in Tables 1 and 2, are consistent with crystallization from crustal-sourced magmas rather than mantle-derived sources. Additionally, the Y/Nb ratio can also help in distinguishing between magmas derived from the mantle and those derived from the continental crust. Mantle-derived sources typically have low Y/Nb ratios (<1.2), while crustal sources exhibit higher Y/Nb ratios (>1.2) [2]. In the case of the Jabal Al Bayda granitic rocks, the average Y/Nb ratios of 2.46 for monzogranites and 1.48 for alkali granites, as reported in Tables 1 and 2, are consistent with a crustal source rather than a mantle source.

The absence of significant evidence of magma mixing in the petrography of the Jabal Al Bayda granitic rocks indeed suggests that magma mixing may not have played a prominent role in their formation. Additionally, the consistent chondrite-normalized REE and trace element patterns observed in all the studied samples, as depicted in Figure 7, further support the idea that the granitic rocks at the Jabal Al Bayda were not formed through a magma mixing process.

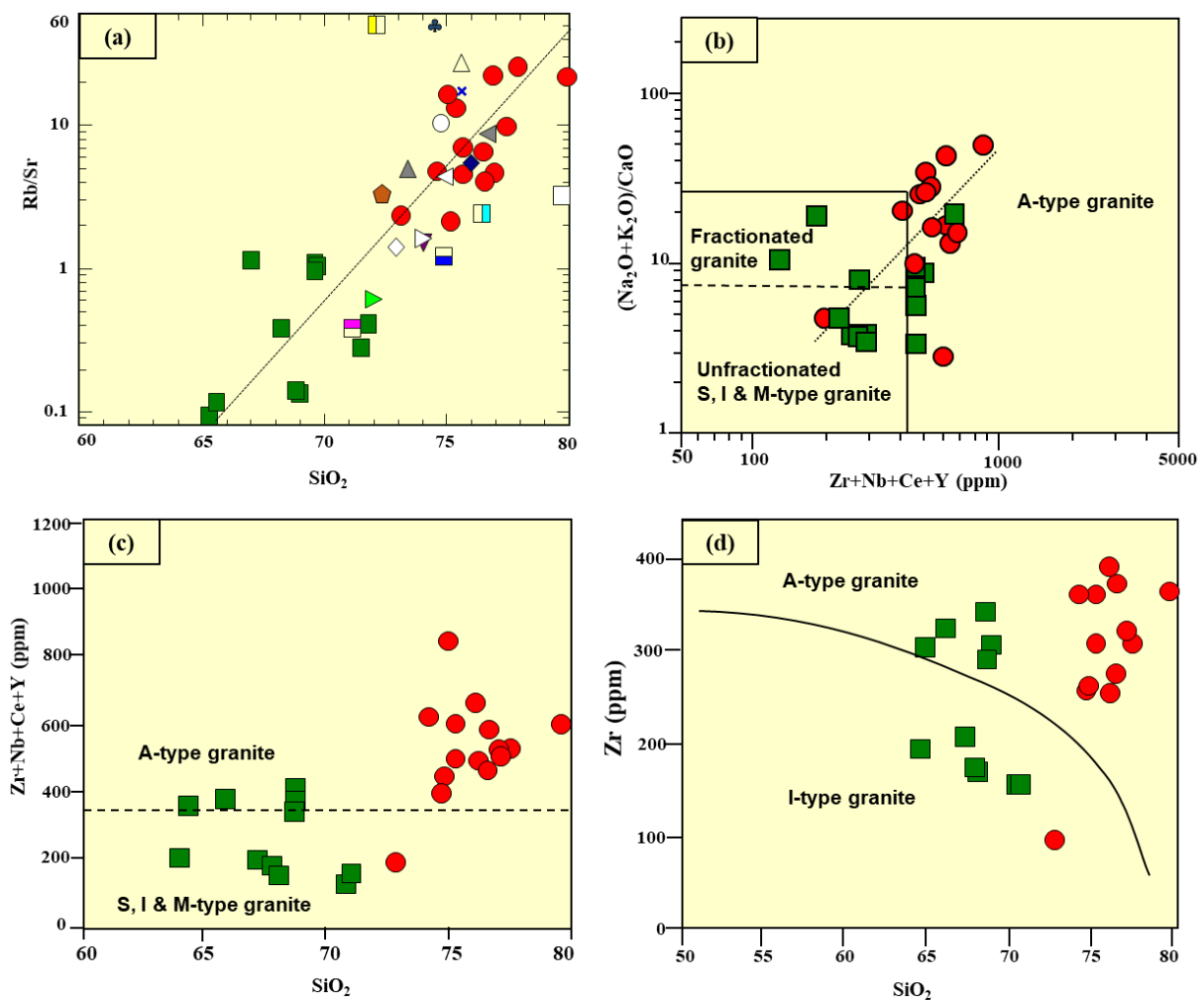


Figure 9. Cont.

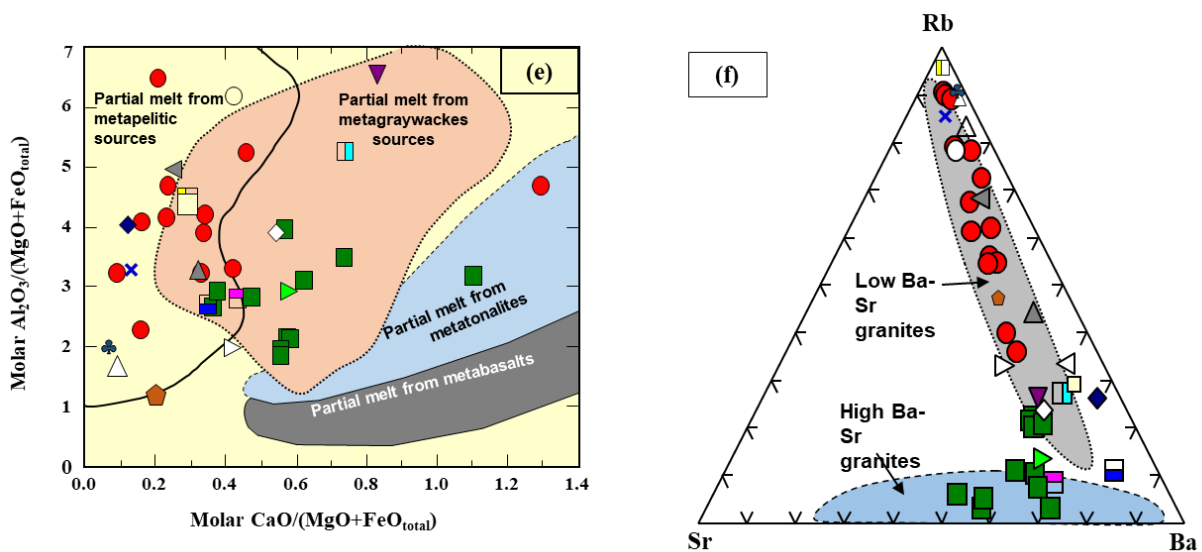


Figure 9. (a) Rb/Sr vs. SiO_2 binary diagram. (b) I-, S-, M-, and A-type granite discrimination diagram after [68]. (c) Zr + Nb + Ce + Y (ppm) versus SiO_2 , with division line of A-type granites from [68]. (d) Zr vs. SiO_2 discrimination diagram for I-type from A-type granitoid rocks [6]. (e) Molar $CaO/(MgO + FeO_{total})$ vs. $Al_2O_3/(MgO + FeO_{total})$ (After [69]). (f) Sr–Rb–Ba ternary plot for the studied granites (modified after [70]). Symbols are as indicated in Figure 6.

As already mentioned, the geochemical compositions of the Jabal Al Bayda granitic plutons show an evolutionary trend from high-K calc-alkaline to alkaline (shoshonite series) types. In the discrimination diagram by [68], the shoshonite series of the alkali granites and monzogranites are plotted as A-type (Figure 9b–d). The high-K calc-alkaline to shoshonite monzogranites are plotted in A-type field and extend into the fractionated felsic I/S/M-granites field. Therefore, we can divide the Jabal al Bayda granitoids into two groups: the high-K calc-alkaline I-type monzogranites, and shoshonite A-type alkali granites and some of monzogranites. The two groups of granites are clearly distinguished in Figure 9b, in which one can also see a trend from older I-types to younger A-types in the studied region.

By plotting the $CaO/(MgO + FeO_{total})$ vs. $Al_2O_3/(MgO + FeO_{total})$ ratios of the studied samples (Figure 9e), it is possible to determine the likely source of the magmas that formed the Jabal Al Bayda granitic rocks. Most of the Jabal Al Bayda granitoids are plotted in metapelite and metagraywackes source fields, supporting a continental crustal source. Tonalite and metasediments as crustal sources were also suggested for numerous alkaline A-type granites in the ANS [43,71]. According to the information provided, it can be concluded that the ‘high-Ca’ monzogranite and ‘low-Ca’ alkali granite at the Jabal Al Bayda have different sources and likely originated from distinct types of protoliths. The ‘high-Ca’ monzogranite is interpreted to represent partial melts of magma derived from clay-poor, plagioclase-rich greywackes sources, with a contribution of tonalitic source, while the ‘low-Ca’ alkali granite is inferred to have originated from metapelitic sources (Figure 9e).

The distinctive geochemical features observed in the monzogranite suite at the Jabal Al Bayda, including enrichment in Sr and Ba but depletion in Rb with low Rb/Sr ratios (Figure 9f), are consistent with characteristics commonly found in high Ba–Sr granitoids (e.g., [72,73]). It is evidenced that almost all of the high Ba–Sr granitic intrusions in the world are located on continental margins [74]. On the contrary, the alkali granite shows the lowest strontium and barium values and the highest Rb contents (178 ppm, on average). The variation in Sr, Ba, and Rb contents in the different granitic types can indeed be influenced by the relative contents of feldspars in these rocks. As evidenced by a petrographical study, the monzogranite is enriched in plagioclase, while alkali granite is high in K-feldspar content. Such differences observed in the monzogranites and alkali granites are similar to

many alkaline intrusions in the ANS (Figure 9f) and can be attributed to a combination of factors, including the composition of the source materials and the conditions under which melting occurs. Ref. [38] studied the isotopic composition of the Jabal az Zuhd granites, in particular, Sr isotopes, and concluded that it was derived from the partial melting of anhydrous metasedimentary lower crust. Ref. [52] investigated the Jabal Sayid granite and interpreted its source to be the result of partial melting of the lower crust of the juvenile AS. Ref. [75] suggested that the source of the Al Ghurayyah granite could be either the mantle or juvenile crust. In Egypt, studies by [33,43,48] focused on different areas such as Wadi Um Sidra, Wadi Al-Baroud, and El Fereyid. They concluded that the monzogranite and alkali feldspar granites in these areas were likely the result of the partial melting of metasedimentary sources or pre-existing granitic crustal rocks.

From the above discussion, the Neoproterozoic granites from the Jabal Al Bayda area could have resulted from the partial melting of diverse metasedimentary and metaigneous sources with variable amounts of metagraywacke, metapelite, and metatonalite source (Figure 9e). The change in tectonic regime from oblique compression to extension can promote the development of steeply inclined shear extension structures within subducted slabs, which can enhance permeability and facilitate the ascent of magma, potentially leading to the formation of high-K calc-alkaline to shoshonite parent magma and A2-type intraplate granites. The sedimentary component of the source material could have originated from two potential sources: (1) During crustal thickening, lower crustal material can be displaced downwards into the mantle. (2) Some sediments can be incorporated and carried with the descending slab during subduction. These sediments can become entrained within the subduction zone and be transported to deeper levels. The depth to which they are carried can vary but can reach depths of 20–30 km [76].

The findings of [53] suggest that A2-type granites can also form in convergent plate boundary settings that are oriented at an angle, rather than orthogonally, to the direction of plate movement. In such cases, slip movements can occur alongside compression strains, creating a transpression regime. In the post-collision and late-collision settings, this transpressive movement can result in feathering extension structures that align with the direction of plate motion. Previous studies by [77,78] have suggested that the resultant magma from A2-type granites is generated through the melting of lower crustal rocks in extensional settings. This is consistent with the formation of post-orogenic alkaline granites in the Arabian Shield. According to [79], the $\epsilon\text{Nd}(T)$ values of the AS range from approximately +4 to +10. These isotopic values suggest that the formation of post-orogenic alkaline granites in the AS involved partial melting of the lower part of the juvenile crust, with or without direct contribution from the upper mantle material. The studies by [45,52,80] further support the idea that the post-orogenic alkaline granites in the AS resulted from the partial melting of the lower crustal rocks. The published geochronologic data indicate that the transition from compressional volcanic arc settings to extensional intraplate settings likely occurred around 650–630 million years ago (Hassan et al., 2016 [78]). This transition coincided with the initiation of the Najd Fault System and the peak metamorphism of the second metamorphic event in the ANS [81].

6.3. Geodynamic Implications

Refs. [82–85] interpreted the evolution of the AS in terms of three main stages of development: (1) The Hijaz orogenic cycle occurred from about 950 to 680 Ma, and involved plate subduction, leading to the formation of the volcanic and associated plutonic rocks in the southern AS. (2) The Nabitah orogeny, occurring from 680 to 630 Ma, represents a significant stage in the tectonic evolution of the AS. During this period, smaller tectonic plates within the AS underwent convergence and collision, leading to the formation of mountain belts and associated intense deformation, and metamorphism of the rocks involved. (3) The Najd orogeny stage occurred from 630 to 550 Ma and involved a period of tectonic deformation and magmatism within the AS. Based on geochemistry and strontium isotope initial ratios, ref. [84] concluded that the volcanic and plutonic rocks in the southern

AS were developed during the Hijaz orogenic cycle. These rocks were formed within intraoceanic island arcs that were associated with northeast-dipping subduction zones. The collision and accretion of the Hijaz and Asir arcs along the Bir Umq suture represent the last stage of the northeast-dipping subduction and collision process.

A different model that interprets the development of the AS during the Pan-African period was proposed by [85]. It was based on three stages as follows: (1) the accretion of oceanic island arcs stage (950–680 Ma), where the development of the Nabitah mobile belt occurred, is considered a suture zone resulting from west-dipping subduction between two allochthonous plates: the western Hijaz-Asir province and the eastern Afif province; (2) a compressional orogeny stage, during the time frame of 680–630 Ma, which occurred as a result of the collision between the Hijaz-Asir and Afif crustal blocks, as well as between the Afif and Ar Rayn crustal blocks; and (3) the final orogenic phase, which occurred from 620 to 550 Ma in the northern Arabian Shield; this phase is characterized by several key geological processes, including extensive molassic sedimentation, granitic plutonism, and the development of the Najd faulting.

In the context of the Jabal Al Bayda area, it is crucial to understand the geodynamic transition that occurred between the termination of subduction-controlled magmatism during the late stages of the East African Orogen and the appearance of post-orogenic granitic magmas. Geochemical similarities between the studied monzogranites and the alkaline stage I (609–602 Ma) of [45] and the 620–600 Ma Idah Suite of [86] suggest a late-orogenic magmatism producing the Jabal Al Bayda monzogranites that occurred at this time. On the other hand, geochemical similarities between the Jabal Al Bayda alkali granites and the 572–556 Ma Feinan A-type granites of [41], the 608–578 Ma alkaline stage II granites of [45], and the 564 ± 140 Ma Jabal az Zuhd granite of [38] suggest a post-orogenic magmatism producing the Jabal Al Bayda Alkali granites that occurred at this time.

Based on the regional geology and magmatic evolutionary history, it is suggested that the Jabal Al Bayda monzogranite was formed through the partial melting of a metagraywacke source within a subduction setting (Figure 10A). This late-orogenic magmatism is believed to have occurred in the range of 620–600 Ma, corresponding to the post-collision stage 3 of the ANS evolution. It follows the accretion of juvenile arc terranes and the formation of volcanic and stratigraphic successions associated with the Al Ays group (745–700 Ma) and the Furayh group (660–630 Ma). The high Ba-Sr signatures of the monzogranite are in agreement with an enriched source related to the partial melting of metagraywackes and metatonalites in a subduction zone. The Jabal Al Bayda A2-type alkali granite shows low Ba-Sr signatures and high Rb content, suggesting a different source and tectonic setting. It is proposed that this alkali granite was formed through partial melting of a metapelitic source in a post-collisional setting (Figure 10B), corresponding to alkaline to peralkaline granite magmatism during the fourth stage of the ANS evolution (~600–530 Ma).

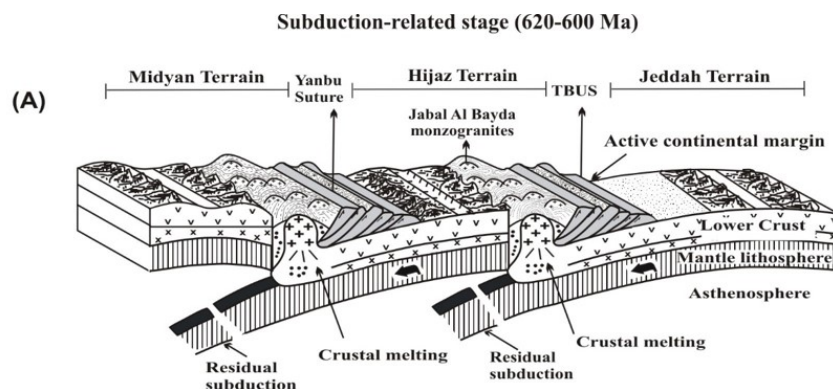


Figure 10. Cont.

Author Contributions: Methodology, H.H.A. and Y.H.D.; Formal analysis, H.H.A. and Y.H.D.; Investigation, H.H.A. and Y.H.D.; Resources, H.H.A.; Data curation, Y.H.D.; Writing—original draft, H.H.A.; Writing—review & editing, H.H.A. and Y.H.D.; Visualization, H.H.A. and Y.H.D.; Supervision, Y.H.D.; Project administration, H.H.A.; Funding acquisition, H.H.A. All authors have read and agreed to the published version of the manuscript.

Funding: This research work was funded by Institutional Fund Projects under grant no. (IFPIP-1443-145-1443).

Institutional Review Board Statement: Not applicable.

Informed Consent Statement: Not applicable.

Data Availability Statement: The data presented in this study is contained within the article.

Acknowledgments: The authors gratefully acknowledge technical and financial support from the Ministry of Education and King Abdulaziz University, Jeddah, Saudi Arabia. We would like to express our gratitude to the reviewers for their valuable comments and suggestions, which have greatly contributed to improving the quality of this manuscript.

Conflicts of Interest: The authors declare no conflict of interest.

References

- Bonin, B. A-type granites and related rocks: Evolution of a concept, problems and prospects. *Lithos* **2007**, *97*, 1–29. [[CrossRef](#)]
- Eby, G.N. Chemical subdivision of the A-type granites: Petrogenetic and tectonic implications. *Geology* **1992**, *20*, 641–644. [[CrossRef](#)]
- Frost, C.D.; Frost, B.R. On ferroan (A-type) granitoids: Their compositional variability and modes of origin. *J. Petrol.* **2011**, *52*, 39–53. [[CrossRef](#)]
- Pearce, J.A.; Harris, N.B.W.; Tindle, A.G. Trace Element Discrimination Diagrams for the Tectonic Interpretation of Granitic Rocks. *J. Petrol.* **1984**, *25*, 956–983. [[CrossRef](#)]
- Anderson, J.L.; Bender, E.E. Nature and origin of Proterozoic A-type granitic magmatism in the southwestern United States. *Lithos* **1989**, *23*, 19–52. [[CrossRef](#)]
- Collins, W.J.; Beams, S.D.; White, A.J.R.; Chappell, B.W. Nature and origin of A-type granites with particular reference to southeastern Australia. *Contrib. Mineral. Petrol.* **1982**, *80*, 189–200. [[CrossRef](#)]
- Bickford, M.E.; Van Schmus, W.R.; Karlstrom, K.E.; Mueller, P.A.; Kamenov, G.D. Mesoproterozoic trans-Laurentian magmatism: A synthesis of continent-wide age distributions, new SIMS U-Pb ages, zircon saturation temperatures, and Hf and Nd isotopic compositions. *Precambrian Res.* **2015**, *265*, 286–312. [[CrossRef](#)]
- Goode, J.W.; Vervoort, J.D. Origin of Mesoproterozoic A-type granites in Laurentia: Hf isotope evidence. *Earth Planet. Sci. Lett.* **2006**, *243*, 711–731. [[CrossRef](#)]
- King, P.L.; White, A.J.R.; Chappell, B.W.; Allen, C.M. Characterization and origin of aluminous A-type granites from the Lachlan Fold Belt, Southeastern Australia. *J. Petrol.* **1997**, *38*, 371–391. [[CrossRef](#)]
- Trumbull, R.B.; Harris, C.; Frindt, S.; Wigand, M. Oxygen and neodymium isotope evidence for source diversity in Cretaceous anorogenic granites from Namibia and implications for A-type granite genesis. *Lithos* **2004**, *73*, 21–40. [[CrossRef](#)]
- Yang, J.-H.; Wu, F.-Y.; Chung, S.-L.; Wilde, S.A.; Chu, M.-F. A hybrid origin for the Qianshan A-type granite, northeast China: Geochemical and Sr–Nd–Hf isotopic evidence. *Lithos* **2006**, *89*, 89–106. [[CrossRef](#)]
- Garfunkel, Z. History and paleogeography during the Pan-African orogen to stable platform transition: Reappraisal of the evidence from Elat area and northern Arabian-Nubian Shield. *Isr. J. Earth Sci.* **2000**, *48*, 135–157.
- Genna, A.; Nehlig, P.; Le Goff, E.; Gguerrot, C.C.; Shanti, M. Proterozoic tectonism of the Arabian Shield. *Precambrian Res.* **2002**, *117*, 21–40. [[CrossRef](#)]
- Stein, M.; Hofmann, A.W. Mantle plumes and episodic crustal growth. *Nature* **1994**, *372*, 63–68. [[CrossRef](#)]
- Stern, R.J.; Hedge, C.E. Geochronologic and isotopic constraints on late Precambrian crustal evolution in the Eastern Desert of Egypt. *Am. J. Sci.* **1985**, *285*, 97–172. [[CrossRef](#)]
- Stern, R.J. Arc assembly and continental collision in the Neoproterozoic East African Orogen: Implications for the consolidation of Gondwanaland. *Annu. Rev. Earth Planet. Sci.* **1994**, *22*, 319–351. [[CrossRef](#)]
- Blades, M.L.; Collins, A.S.; Foden, J.; Payne, J.L.; Xu, X.; Alemu, T.; Woldetinsae, G.; Clark, C.; Taylor, R.J.M. Age and hafnium isotopic evolution of the Didesa and Kemashi Domains, western Ethiopia. *Precambrian Res.* **2015**, *270*, 267–284. [[CrossRef](#)]
- Fritz, H.; Abdelsalam, M.; Ali, K.A.; Bingen, B.; Collins, A.S.; Fowler, A.R.; Ghebreaab, W.; Hauenberger, C.A.; Johnson, P.R.; Kusky, T.M.; et al. Orogen styles in the East African Orogen: A review of the Neoproterozoic to Cambrian tectonic evolution. *J. Afr. Earth Sci.* **2013**, *86*, 65–106. [[CrossRef](#)]
- Worku, H.; Schandlmeier, H. Tectonic evolution of the Neoproterozoic Adola Belt of southern Ethiopia: Evidence for a Wilson Cycle process and implications for oblique plate collision. *Precambrian Res.* **1996**, *77*, 179–210. [[CrossRef](#)]
- Stern, R.J.; Gottfried, D.; Hedge, C.E. Late Precambrian Rifting and Crustal Evolution in the Northeastern Desert of Egypt. *Geology* **1984**, *12*, 168–172. [[CrossRef](#)]

21. Al-Shanti, A.M.S.; Pint, J.J.; Al-Juaid, A.J.; Al-Amoudi, S.A. *Preliminary Survey for Caves in the Habakah Region of the Kingdom of Saudi Arabia. Saudi Geological Survey Open-File Report SGS-OF*; Saudi Geological Survey: Jeddah, Saudi Arabia, 2003; 32p.
22. Johnson, P.R.; Andresen, A.; Collins, A.S.; Fowler, A.R.; Fritz, H.; Ghebreab, W.; Kusky, T.; Stern, R.J. Late Cryogenian-Ediacaran history of the Arabian-Nubian Shield: A review of depositional, plutonic, structural, and tectonic events in the closing stages of the northern East African Orogen. *J. Afr. Earth Sci.* **2011**, *61*, 167–232. [[CrossRef](#)]
23. Stoesser, D.B.; Frost, C.D. Nd, Pb, Sr, and O isotopic characteristics of Saudi Arabian shield terrains. *Chem. Geol.* **2006**, *226*, 163–188. [[CrossRef](#)]
24. Al-Shanti, A.M.S. *The Geology of the Arabian Shield: General Geology*; King Abdulaziz University Press: Jeddah, Saudi Arabia, 2003; Volume 3–7, 204p.
25. Brosset, R. *Geology and Mineral Exploration of the Al-Madinah Quadrangle, 24/39D*; Bureau de Recherches Géologiques et Minières (BRGM): Jeddah, Saudi Arabia, 1976.
26. Johnson, P.R. *Explanatory Notes to the Map of Proterozoic Geology of Western Saudi Arabia. Saudi Geological Survey Technical Report SGS-TR-2006-4*; Saudi Geological Survey: Jeddah, Saudi Arabia, 2006; p. 62, 22 Figures, 2 Plates.
27. Johnson, P.R.; Halverson, G.P.; Kusky, T.M.; Stern, R.J.; Pease, V. Volcanosedimentary Basins in the Arabian-Nubian Shield: Markers of repeated exhumation and denudation in a Neoproterozoic accretionary orogen. *Geosciences* **2013**, *3*, 389–445. [[CrossRef](#)]
28. Pellaton, C. *Geologic Map of the Al Madinah Quadrangle, Sheet 24D*; Saudi Arabian Deputy Ministry for Mineral Resources Geoscience Map Series; Geo Map GM-52; Ministry of Petroleum and Mineral Resources; Deputy Ministry for Mineral Resources: Jeddah, Saudi Arabia, 1981; 19p.
29. Sakr, S.M.; Bamousa, A.O.; Gad, A. Nb-Zr enrichment in Jabal Al Bayda A-type granites, western Arabian Shield, Saudi Arabia: Interplay of magmatic and hydrothermal processes. *J. Taibah Univ. Sci.* **2022**, *16*, 505–524. [[CrossRef](#)]
30. De La Roche, H.; Leterrier, J.; Grandelaude, P.; Marchal, M. A classification of volcanic and plutonic rocks using R1R2-diagram and major-element analyses—Its relationships with current nomenclature. *Chem. Geol.* **1980**, *29*, 183–210. [[CrossRef](#)]
31. Maniar, P.D.; Piccoli, P.M. Tectonic discrimination of granites. *Geol. Soc. Am. Bull.* **1989**, *101*, 635–643. [[CrossRef](#)]
32. Awad, A.A.; Abu El-Leil, A.; Nastavkin, A.V.; Tolba, A.; Kamel, M.; El-Wardany, R.M.; Rabie, A.; Ene, A.; Tekin, H.O.; Issa, S.A.M.; et al. Statistical analysis on the radiological assessment and geochemical studies of granite rocks in the north of Um Taghir area, Eastern Desert, Egypt. *Open Chem.* **2022**, *20*, 254–266. [[CrossRef](#)]
33. Saleh, G.M.; Afify, A.M.; Emad, B.M.; Dawoud, M.I.; Shahin, H.A.; Khaleal, F.M. Mineralogical and geochemical characterization of radioactive minerals and rare earth elements in granitic pegmatites at G. El Fereyid, South Eastern Desert, Egypt. *J. Afr. Earth Sci.* **2019**, *160*, 103651. [[CrossRef](#)]
34. Wright, J.B. A simple alkalinity ratio and its application to questions of non-orogenic granite genesis. *Geol. Mag.* **1969**, *106*, 370–384. [[CrossRef](#)]
35. Peccerillo, A.; Taylor, S.R. Geochemistry of Eocene calcalkaline volcanic rocks from the Kastamonu area, northern Turkey. *Contrib. Miner. Petrol.* **1976**, *58*, 63–81. [[CrossRef](#)]
36. Frost, B.R.; Barnes, C.G.; Collins, W.J.; Arculus, R.J.; Ellis, D.J.; Frost, C.D. A geochemical classification for granitic rocks. *J. Petrol.* **2001**, *42*, 2033–2048. [[CrossRef](#)]
37. Robinson, F.A.; Foden, J.D.; Collins, A.S. Geochemical and isotopic constraints on island arc, synorogenic, post-orogenic and anorogenic magmatism in the Arabian Shield, Saudi Arabia. *Lithos* **2015**, *220–223*, 97–115. [[CrossRef](#)]
38. Bakhsh, R.A.M. *Granites from the Midyan Terrain, NW Saudi Arabia: Petrology, Geochemistry and Geochronology*. Ph.D. Thesis, Royal Holloway, University of London, Egham, UK, 2013; 250p.
39. Qadhi, T.M. Origin and hydrothermal alteration of rare-metal granites in the Al-Hamra area, northeastern Arabian Shield, Saudi Arabia. *Cent. Eur. Geol.* **2007**, *50/3*, 259–282. [[CrossRef](#)]
40. Aseri, A.A. *Rare-Metal Alkaline Granite from the Arabian Shield, Saudi Arabia*. Ph.D. Thesis, Electronic Thesis and Dissertation Repository. The University of Western Ontario, London, ON, Canada, 2020; p. 6822. Available online: <https://ir.lib.uwo.ca/etd/6822> (accessed on 1 March 2020).
41. Jarrar, G.H.; Manton, W.I.; Stern, R.J.; Zachmann, D. Late Neoproterozoic A-type granites in the northernmost Arabian-Nubian Shield formed by fractionation of basaltic melts. *Geochemistry* **2008**, *68*, 295–312. [[CrossRef](#)]
42. Mohamed, H.A.; Ali, S.; Sedki, T.; Abdel Khalik, I.I. The Sukari Neoproterozoic granites, Eastern Desert, Egypt: Petrological and structural implications. *J. Afr. Earth Sci.* **2019**, *149*, 426–440. [[CrossRef](#)]
43. El-Bialy, M.Z.; Omar, M.M. Spatial association of Neoproterozoic continental arc I-type and post-collision A-type granites in the Arabian–Nubian Shield: The Wadi Al-Baroud Older and Younger Granites, North Eastern Desert, Egypt. *J. Afr. Earth Sci.* **2015**, *103*, 1–29. [[CrossRef](#)]
44. Abdalla, H.M. Mineralogical and geochemical characterization of beryl-bearing granites, Eastern Desert, Egypt: Metallogenic and exploration constraints. *Resour. Geol.* **2009**, *59*, 121–139. [[CrossRef](#)]
45. Eyal, M.; Litvinovsky, B.; Jahn, B.M.; Zanvilevich, A.; Katzir, Y. Origin and evolution of post-collisional magmatism: Coeval Neoproterozoic calc-alkaline and alkaline suites of the Sinai Peninsula. *Chem. Geol.* **2010**, *269*, 153–179. [[CrossRef](#)]
46. McDonough, W.F.; Sun, S. The composition of the Earth. *Chem. Geol.* **1995**, *120*, 223–253. [[CrossRef](#)]
47. Harris, N.B.W.; Pearce, J.A.; Tendle, A.G. Geochemical Characteristics of Collision-Zone Magmatism. *Geol. Soc. Lond. Spec. Publ.* **1986**, *19*, 67–81. [[CrossRef](#)]

48. El Afandy, A.H.; El Kalioubi, B.A.; Eliwa, H.A.; Khamis, H.A.; Seddiek, S.H. Geological, geochemical, and petrogenetic aspects of Late Neoproterozoic younger granites at Wadi Um Sidra-Wadi Um Asmer area, North Eastern Desert. *Egypt. J. Geol.* **2020**, *64*, 297–312.
49. Schandle, E.S.; Groton, M.P. Application of high field strength elements to discriminate tectonic settings in VMS environments. *Econ. Geol.* **2002**, *97*, 629–642. [[CrossRef](#)]
50. Thiéblemont, D.; Tegye, M. Une discrimination géochimique des Roches différenciées témoin de la diversité d'origine et de situation Tectonique des magmas calco-alkalins. *Comptes Rendus L'Académie Sci. Paris* **1994**, *319*, 87–94.
51. Ghoneim, M.F.; Lebda, E.M.; Abu Anbar, M.M. Further geochemical and mineralogical discrimination between granitic rocks of the Eastern Desert of Egypt. In *Proceedings of the 4th International Conference on Geology Arab World*; Cairo University: Giza, Egypt, 1999; pp. 266–286.
52. Moghazi, A.K.M.; Iaccheri, L.M.; Bakhsh, R.A.; Kotov, A.B.; Ali, K.A. Sources of rare-metal-bearing A-type granites from Jabel Sayed complex, northern Arabian shield, Saudi Arabia. *J. Asian Earth Sci.* **2015**, *107*, 244–258. [[CrossRef](#)]
53. Grebennikov, A.V. A-type granites and related rocks: Petrogenesis and classification. *Russ. Geol. Geophys.* **2014**, *55*, 1074–1086. [[CrossRef](#)]
54. Brophy, J.G. Composition gaps, critical crystallinity, and fractional crystallization in orogenic (calc-alkaline) magmatic systems. *Contrib. Mineral. Petrol.* **1991**, *109*, 173–182. [[CrossRef](#)]
55. Brophy, J.G. A study of rare earth element (REE)-SiO₂ variations in felsic liquids generated by basalt fractionation and amphibolite melting: A potential test for discriminating between the two different processes. *Contrib. Mineral. Petrol.* **2008**, *156*, 337–357. [[CrossRef](#)]
56. Ingle, S.; Weis, D.; Scoates, J.S.; Frey, F.A. Relationship between the early Kerguelen plume and continental flood basalts of the paleo-Eastern Gondwanan margins. *Earth Planet. Sci. Lett.* **2002**, *197*, 35–50. [[CrossRef](#)]
57. Macpherson, C.G.; Dreher, S.T.; Thirlwall, M.F. Adakites without slab melting: High pressure processing of basaltic island arc magma, Mindanao, the Philippines. *Earth Planet. Sci. Lett.* **2006**, *243*, 581–593. [[CrossRef](#)]
58. Streck, M.J.; Leeman, W.P.; Chesley, J. High-magnesian andesite from Mount Shasta: A product of magma mixing and contamination, not a primitive mantle melt. *Geology* **2007**, *35*, 351–354. [[CrossRef](#)]
59. Huang, J.X.; Gréau, Y.; Griffin, W.L.; O'Reilly, S.Y.; Pearson, N.J. Multi-stage origin of Roberts Victor eclogites: Progressive metasomatism and its isotopic effects. *Lithos* **2012**, *142–143*, 161–181. [[CrossRef](#)]
60. Peng, T.P.; Zhao, G.C.; Fan, W.M.; Peng, B.X.; Mao, Y.S. Zircon geochronology and Hf isotopes of Mesozoic intrusive rocks from the Yidun terrane, Eastern Tibetan Plateau: Petrogenesis and their bearings with Cu mineralization. *J. Asian Earth Sci.* **2014**, *80*, 18–33. [[CrossRef](#)]
61. Wang, Q.; Wyman, D.A.; Li, Z.; Bao, Z.; Zhao, Z.; Wang, Y.; Jian, P.; Yang, Y.; Chen, L. Petrology, geochronology and geochemistry of ca. 780 Ma A-type granites in South China: Petrogenesis and implications for crustal growth during the breakup of the supercontinent Rodinia. *Precambrian Res.* **2010**, *178*, 185–208. [[CrossRef](#)]
62. Wu, R.X.; Zheng, Y.F.; Wu, Y.B.; Zhao, Z.F.; Zhang, S.B.; Liu, X.M.; Wu, F.Y. Reworking of juvenile crust: Element and isotope evidence from Neoproterozoic granodiorite in South China. *Precambrian Res.* **2006**, *146*, 179–212. [[CrossRef](#)]
63. Wu, F.Y.; Yang, Y.H.; Xie, L.W.; Yang, J.H.; Xu, P. Hf isotopic compositions of the standard zircons and baddeleyites used in U–Pb geochronology. *Chem. Geol.* **2006**, *234*, 105–126. [[CrossRef](#)]
64. Xiao, L.; Zhang, H.F.; Ni, P.-Z.; Xiang, H.; Liu, X.M. LA-ICP-MS U–Pb zircon geochronology of early Neoproterozoic mafic-ultramafic intrusions from NW margin of the Yangtze Block, South China: Implication for tectonic evolution. *Precambrian Res.* **2007**, *154*, 221–235. [[CrossRef](#)]
65. Taylor, S.R.; McLennan, S.M. *The Continental Crust: Its Composition and Evolution*; Blackwell Scientific Publications: Oxford, UK, 1985; 312p, ISBN 978-0632011483.
66. Rudnick, R.L.; Fountain, D.M. Nature and composition of the continental crust: A lower crustal perspective. *Rev. Geophys.* **1995**, *33*, 267–309. [[CrossRef](#)]
67. Green, T.H. Significance of Nb/Ta as an indicator of geochemical processes in the crust mantle system. *Chem. Geol.* **1995**, *120*, 347–359. [[CrossRef](#)]
68. Whalen, J.B.; Currie, K.L.; Chappell, B.W. A-type granites: Geochemical characteristics, discrimination and petrogenesis. *Contrib. Mineral. Petrol.* **1987**, *95*, 407–419. [[CrossRef](#)]
69. Gerdes, A.; Montero, P.; Bea, F.; Fershter, G. Peraluminous granites frequently with mantle-like isotope compositions: The continental-type Murzinka and Dzhabyk batholiths of the eastern Urals. *Int. J. Earth Sci.* **2002**, *91*, 3–19. [[CrossRef](#)]
70. Tarney, J.; Jones, C.E. Trace element geochemistry of orogenic igneous rocks and crustal growth models. *J. Geol. Soc. Lond.* **1994**, *151*, 855–868. [[CrossRef](#)]
71. Sami, M.; Ntaflos, T.; Farahat, E.S.; Mohamed, H.A.; Ahmed, A.F.; Hauzenberger, C. Mineralogical, geochemical and Sr–Nd isotopes characteristics of fluorite-bearing granites in the Northern Arabian-Nubian Shield, Egypt: Constraints on petrogenesis and evolution of their associated rare metal mineralization. *Ore Geol. Rev.* **2017**, *88*, 1–22. [[CrossRef](#)]
72. Jiang, Y.D.; Sun, M.; Kröner, A.; Tumurkhuu, D.; Long, X.P.; Zhao, G.C.; Yuan, C.; Xiao, W.J. The high-grade Tsel Terrane in SW Mongolia: An Early Paleozoic arc system or a Precambrian sliver? *Lithos* **2012**, *142*, 95–115. [[CrossRef](#)]
73. Peng, T.P.; Wilde, S.A.; Fan, W.M.; Peng, B.X. Late Neoproterozoic potassic high Ba–Sr granites in the Taishan granite–greenstone terrane: Petrogenesis and implications for continental crustal evolution. *Chem. Geol.* **2013**, *344*, 23–41. [[CrossRef](#)]

74. Zhang, Y.; Sun, M.; Yuan, C.; Xu, Y.; Long, X.; Tomurhuu, D.; Wang, C.Y.; He, B. Magma mixing origin for high Ba–Sr granitic pluton in the Bayankhongor area, central Mongolia: Response to slab roll-back. *J. Asian Earth Sci.* **2015**, *113*, 353–368. [[CrossRef](#)]
75. Qadhi, T.; Moufti, A. Geochemical characteristic of the rare-metal rich granite in the Ghurayyah-Dubbagh Area, north western Arabian Shield, Saudi Arabia. *Ann. Geol. Surv. Egypt* **2008**, *XXX*, 149.
76. Karig, D.E.; Kay, R.W. Fate of sediments on the descending plate at convergent margins. *Phil. Trans. R. Soc. Lond.* **1981**, *301*, 233–251.
77. Abu-Alam, T.S.; Stüwe, K. Exhumation during oblique transpression: An example from the Feiran–Solaf region, Egypt. *J. Metamorph. Geol.* **2009**, *27*, 439–459. [[CrossRef](#)]
78. Hassan, M.; Abu-Alam, T.S.; Hauzenberger, C.; Stüwe, K. Geochemical signature variation of Pre-, Syn- and Post-shearing intrusives within the Najd Fault System of Western Saudi Arabia. *Lithos* **2016**, *263*, 274–291. [[CrossRef](#)]
79. Moghazi, A.M.; Ali, K.A.; Wilde, S.A.; Zhou, Q.; Andersen, T.; Andresen, A.; El-enen, M.M.A.; Stern, R.J. Geochemistry, geochronology, and Sr–Nd isotopes of the Late Neoproterozoic Wadi Kid volcano-sedimentary rocks, Southern Sinai, Egypt: Implications for tectonic setting and crustal evolution. *Lithos* **2012**, *154*, 147–165. [[CrossRef](#)]
80. Ali, K.A.; Jeon, H.; Andresen, A.; Li, S.Q.; Harbi, H.M.; Hegner, E. U–Pb zircon geochronology and Nd–Hf–O isotopic systematics of the Neoproterozoic Hadb adh Dayheen ring complex, Central Arabian Shield, Saudi Arabia. *Lithos* **2014**, *206–207*, 348–360. [[CrossRef](#)]
81. Abu-Alam, T.S.; Hassan, M.; Stüwe, K.; Meyer, S.E.; Passchier, C.W. Multistage tectonism and metamorphism during Gondwana collision: Baladiyah Complex, Saudi Arabia. *J. Petrol.* **2014**, *55*, 1941–1964. [[CrossRef](#)]
82. Brown, G.B. *Tectonic Map of the Arabian Peninsula*; Saudi Arabian Directorate General of Mineral Resources Map, Scale 1:4,000,000; U.S. Geological Survey: Reston, VA, USA, 1972.
83. Greenwood, W.R.; Anderson, R.E.; Fleck, R.J.; Robert, R.J. Precambrian geologic history and plate tectonic evolution of the Arabian Shield. *Saudi Arab. Dir. Miner. Resour. Bull.* **1980**, *24*, 35.
84. Greenwood, W.R.; Hadley, D.G.; Anderson, R.E.; Fleck, R.J.; Schmidt, D.L. Late Proterozoic cratonization in southwestern Saudi Arabia. *Philos. Transact. R. Soc. Lond. Ser. A* **1976**, *280*, 517–527.
85. Stoeser, D.B.; Jackson, N.J.; Ramsay, C.R.; Drysdall, A.R.; Du Bray, E.A.; Douch, C.J. Map of felsic plutonic rocks in the Arabian Shield, Kingdom of Saudi Arabia. 1:1000000 (2 sheets). *J. Afr. Earth Sci.* **1986**, *4*.
86. Robinson, F.A.; Foden, J.D.; Collins, A.S.; Payne, J.L. Arabian Shield magmatic cycles and their relationship with Gondwana assembly: Insights from zircon U–Pb and Hf isotopes. *Earth Planet. Sci. Lett.* **2014**, *408*, 207–225. [[CrossRef](#)]

Disclaimer/Publisher’s Note: The statements, opinions and data contained in all publications are solely those of the individual author(s) and contributor(s) and not of MDPI and/or the editor(s). MDPI and/or the editor(s) disclaim responsibility for any injury to people or property resulting from any ideas, methods, instructions or products referred to in the content.